A New Look at the Pacific Storm Track Variability: Sensitivity to Tropical SSTs and to Upstream Seeding

by
Isidoro Orlanski

Geophysical Fluid Dynamics Laboratory/ NOAA
Forrestal Campus, Princeton University
Princeton, NJ 08542

March 15, 2004

Abstract.

There is a fairly well defined response of the stationary wave and storm track over the Pacific to El-Nino SSTs. In this paper, the case is made that this response is primarily a result of increased baroclinicity in the central Pacific, with changes in stationary wave pattern farther east mainly forced by changes in these transient eddies. There is also a lot of natural variability that is not associated with El-Nino. This paper makes the case that much of the variability can be understood as forced by variations in the upstream seeding of the storm track. The paper does not address the question of whether these variations in seeding should be thought of as chaotic noise or as themselves forced by identifiable mechanisms. Thus, the claim is that there are two key parameters mid-Pacific baroclinicity, controlled by SST's and the strength of the upstream seeding.

The discussion on the effect of storm track seeding by waves entering from the Asian continent first focuses on the normal years. The results show that two mechanisms operate to distribute the eddy energy along the storm track: downstream development and baroclinic development. The large effect on baroclinic development at the storm track entrance is due to a combination of different factors, surface baroclinicity, land-sea contrast and strong moist fluxes from the western subtropics. Waves entering the storm track from the cold continent receive a considerable amount of surface heat fluxes that energizes them, and the fact that a large amount of moisture exists in normal years on the western subtropics is an extra source for wave growth. Sensitivity to the seeding

amplitude in the experiments is large. The larger the seeding amplitude is, the closer the more intense baroclinic waves flux energy downstream to upper level waves. These waves become more barotropic because in normal years the baroclinicity on the mid-Pacific region is rather weak. These barotropic waves tend to break anticyclonicaly and produce the ridge in the eastern Pacific.

The sensitivity to SST anomalies shows qualitative and quantitative similarity with the observed anomalies. These simulations show increased baroclinicity in the mid-Pacific because that stronger convection in the mid-tropical Pacific enhances a large pool of warm air over the entire mid-eastern subtropical ocean. The pool of warm air is the source of enhanced baroclinicity in the region. This eastward displacement of the baroclinic zone in El Nino years produces an extra source for baroclinic development in the mid-eastern Pacific Ocean, which tend to reduce the effects over the PNA region of the waves originating at the entrance of the storm track. However, the waves with sources at the storm track entrance break anticyclonically and produce the ridge in the eastern Pacific. The baroclinic waves generated or regenerated in the middle of the ocean tend to break cyclonically, produce a trough tendency and reduce the amplitude of the eastern ridge.

These results strongly suggest that: a) the variability of the quasi-permanent circulation could indeed be produced by the high frequency eddy feedback. b) Two main

mechanisms operate for the forcing of the quasi-permanent circulation; *downstream development* from the western ocean and the anomalous *baroclinicity in the mid-eastern Pacific. The intensity of these two counteracting forcings gives the different flavors of the EL NINO response over the PNA region. It should be noted that regardless of weak and strong SST anomalies, the PNA patterns seem unique but obviously have different intensities.*

1. Introduction

Despite the large number of articles devoted to the role of tropical SST s in the variability of the northern winter Pacific storm track, the topic remains controversial (see Hoerling and Kumar 2002, hereafter HK02, for an extended reference). In a very complete discussion of the extratropical response over the Pacific North America region (PNA) variability and its relation with tropical SSTs and in particular with ENSO variability (HK02) the authors concluded that: it seems clear that the existence of a teleconnection pattern forced by changes in tropical SSTs is associated with El Nino-Southern Oscillation (ENSO). However, they also noted that the variations of the different flavors in the response of the extratropical atmosphere for different El Ninos are quite large. It is more or less an accepted fact that the year-to-year PNA sector variability explained by ENSO is indeed limited by the intrinsic atmospheric variability. Observed seasonal anomalies during different El Ninos are often distinct from each other, though contrary interpretations have been offered. Madden (1976) proposed that the variability of observed monthly sea level pressure is due to the internal atmospheric variations attributable to daily weather fluctuations and is not caused by sensitivity to boundary forcing. This argument has been supported by results from general circulation models (Geisler et al. 1985, Kumar and Hoerling 1997) that find only a weak extratropical sensitivity to changes in tropical Pacific SSTs from event to event. However, a contradictory argument, offered by Palmer and Owen (1986), was that the inter-El Nino

differences in the extratropical seasonal anomaly can be explained by SST variations supporting the contention that a substantial signal exists in the extratropics, but which varies from one ENSO event to another (Trenberth 1993). In the HK02 review, the authors analyzed the results of a large number of ensemble atmospheric climate simulations forced with the modern record of interannually varying tropical forcing and concluded that the observed estimate of the fraction of year-to-year PNA sector variability explained by ENSO is indeed limited by the intrinsic atmospheric variability. Further, much of the ENSO response itself is manifested as a single spatial pattern as they mention, other patterns were identified, however they contributed a very small signal over the PNA sector as a whole. Although it seems clear what the origin of the tropical forcing is, the so called atmospheric variability is considerably more obscure. Simmons et al. (1983) suggested that low frequency barotropic waves of 30 to 50 days periods, generated by barotropic instability could be the cause determining the response to anomalous boundary forcing, such as tropical SSTs. It is rather well known that high frequency baroclinic eddies can have a significant role in shaping the Pacific storm track (Lau and Nath 1991, Orlanski 1998, Chang et al 2002, among others). Moreover, Orlanski (1998), analyzing the barotropic forcing exerted by the baroclinic eddies over two ENSO cycles, suggested that the quasi stationary response of the upper level heights has strong similarities with the observed PNA pattern. More recently, Orlanski (2003) found a very suggestive result that the intensity of high frequency low level baroclinic waves can force

the upper level waves in such a way that for low-amplitude forcing the upper level waves break anticyclonically, moving the jet poleward. **A**s the forcing is enhanced, this mechanism is intensified: stronger low level eddies push the upper level jet farther north. Furthermore, eddy intensification produces a drastic change in the breaking of the upper level waves, making them break cyclonically and consequently, the jet is pushed equatorward. Since this shift in the behavior depends on reaching a critical energy level that depends on the horizontal scale of the waves, frequently short baroclinic waves will reach the threshold to break cyclonically, whereas the longer waves require much more energy to produce the shift. Then we can conclude that the bifurcation of eddy life cycles has a bearing on the interannual variability of storm tracks. In Non- El Nino years, waves entering from eastern Asia to the Pacific storm track region will be enhanced by baroclinic development at the entrance of the storm track, dispersed by downstream flux of energy and develop a more barotropic upper level wave since the middle Pacific is depleted of most of its baroclinicity (Chang and Orlanski 1993). Finally, the barotropic waves break anticyclonically in the eastern Pacific. In El Nino years, as the convective regions move to the mid-Pacific, enhanced baroclinicity in the subtropics could enhance baroclinic development further eastward and support more intense shorter waves that will eventually break cyclonically and maintain the subtropical jet eastward.

Given the large amount of work on this topic (HK02, Kushnir 2002, among others), it seems clear that although the mechanisms are not well understood, the sensitivity of the

extratropical response to anomalous tropical SSTs has considerable variability and it appears to be the combined role of the boundary forcing (through the tropical SSTs) and the internal atmospheric variability that are responsible for such behavior.

The work that we will present is quite distinct from the many articles written on the subject. First, a high resolution nonhydrostatic cloud resolving model will be used to simulate the Pacific storm track and its sensitivity to tropical SSTs and natural variability. The experiments have been designed to treat the natural variability and the effect of tropical SSTs anomalies independently. Our premise is simple; it assumes that most of the variability is connected one way or another to the high frequency eddy activity in the storm track (Orlanski 1998, 2003). Then, our goal is to assess: first, how much the natural variability, measured as high frequency waves entering the west Pacific storm track, can affect the response in the storm track; second, how tropical anomalous SSTs can produce the well known response in the PNA region; and finally, how the natural variability interferes with the surface boundary forcing to provide a great variability in the storm track response in the PNA region. In Section 2 we will describe the model and experimental setting; in Section 3 the control solution will be presented and Section 4 will discuss the changes due to natural variability**.** Section 5 will present the storm track response to tropical heating anomalies and the summary and conclusions will be in Section 6.

2 Model and Methodology

The solutions were obtained by integrating a compressible nonhydrostatic high resolution ZETAC[1] model (9km and 18km horizontal resolutions in the storm track region, see Appendix). The area of the simulations is the entire North Pacific Ocean from 120E to 85W and 3S to 82.5N. Other model characteristics include a terrain following coordinate that extends from the surface to around 25 km height and an explicit moist convection with a simple Kessler microphysics parameterization. The regional model is forced only at the western boundary. The entrance of the storm track by a climatological jet is shown in Fig 1 and the forcing at the lower ocean boundary by prescribing SSTs is shown in Fig 2. Integrating the model for 220 days and analyzing the last 50 days provides the control solution.

Since our goal is to evaluate two independent effects: the natural variability and the tropical SST anomaly affecting the storm track response in the PNA sector, we will perform sensitivity experiments by initializing different sensitivity runs at day140 of the control, run the solution to 220 days and compare the last fifty days of each solution to the control. Testing the sensitivity to SSTs is rather simple. Using the SST shown in Fig 2 we include an anomaly in the tropics mimicking El Nino SSTs (we have used a couple of slightly different SSTs to reflect weak and strong EL Nino events). For evaluating the natural variability, we assume that most of the variability is generated by wave activity

1The ZETAC model (developed by Dr. Steve Garner) is written using GFDL's Flexible Modeling System (FMS)

from Asia at the storm track entrance. Therefore, we nudge the zonal and meridional velocities at the western boundary with an upper level wave in which the amplitude and frequency are random. We fix the STD of the forced amplitude to values close to the observed values for winter conditions. Two STD values were used to characterize the wave noise, 5m/s (*moderate*) and 8m/s (*strong*); the random period fluctuated from 3 to 5 days. These rather high frequency forcings were intentional to ascertain whether any low frequency response in this simulation originated from a high frequency forcing. No other boundary or interior forcing has been applied. Since it is assumed that considerable feedback is from the high frequency eddies that modify the large scale flow in the storm track, we wanted the model to freely determine its large scale circulation rather than be forced to a prescribed one.

3. The control solution:

As previously mentioned, the Control ran for 220 days and the last 50 days were analyzed. Fig 3 shows the time averaged variables of the Control solution. On the left we show the upper level zonal component of the wind at 8900m (upper) and the time averaged surface potential temperature (lower); the remaining panels on the right show water vapor (lower) and the pressure deviations from the zonal distribution at the intiation (day 170) of the sensitivity runs (upper). The time mean distribution of these quantities seems very realistic; this is particularly true for the jet intensification in the western

Pacific and the poleward deflection in the eastern Pacific. It is a classical picture of the trough-ridge associated with the storm track (Orlanski 1998); the magnitude and poleward displacement of the subtropical jet seem very realistic for winter time conditions. The other fields also seem very well resolved, especially the intensification of the moist-thermodynamic variables in the tropical western region. The precipitation is coincident with the tongue of the warm surface temperatures in the western equatorial ocean. The time mean pressure perturbation of the zonal pressure (upper panel) displays a trough in the mid-Pacific Ocean bounded by two ridges with the most intense ridge over the PNA sector. However, notice that although the ridge position correlates well with observations, the observations also show that the trough starts at the entrance of the storm track and extends east of the dateline. This trough actually is generated by two distinct processes: the Tibetan Plateau and the baroclinic eddy feedback. The large orography produces a trough on the lee of the plateau extending to the western Pacific Ocean (Held et al: 2002) and the feedback from baroclinic eddies produces a trough around the middle of the storm track (Lau and Nath 1991 and Orlanski 1998). The effect of the Tibetan Plateau certainly is missing from our experimental design but it does not detract from the generalities of the conclusions. The downstream intensity of the trough displayed in the figure will be discussed shortly. Fig 4 shows the variance of the upper level meridional velocity for the DEC-JAN climatology of the NCEP-NCAR reanalysis**.** The middle panel shows the time averaged variance for the Control with moderate seeding; this will be the reference solution used throughout the paper, and at the bottom, a solution with

conditions similar to the Control but with strong seeding on the western boundary. Occasionally throughout the paper we will show some climatology from the NCEP-NCAR Reanalysis (16 years from 1983) similar to that shown in Fig 4. We need to stress the fact that neither the mean flow nor the SSTs are, in the simulations, from real data; only the topography is real and showing a comparison with climatology could be misleading. However, since this paper relies heavily on the intensity of the high frequency baroclinic eddies, it would be instructive to show the observed variance and see that we are in the realm of realistic simulations. Actually, the similarities and energy levels are quite striking**.** An in depth discussion on the upstream seeding appears in the next section.

4. Sensitivity to natural variability:

First, let us review the factors that determine the baroclinic eddy feedback in normal (Non-EL Nino) years to the quasi-stationary circulation (Orlanski 1998, 2003) before embarking on the description of the effects due to a change in the tropical SSTs. Two main mechanisms complement each other to give variability in the strength of the eastern ridge at the termination of the storm track:

a· the variability of the intensity and number of eddies from the Siberian storm track reaching the warm waters of the Pacific Ocean

b· the relation of the intensity of the anticyclonic wave breaking with the

poleward deflection of the storm track axis .

a) The seeding and downstream development:

Orlanski (1998) suggests that one possible explanation for the so-called midwinter suppression (Nakamura 1992) is the reduced intensity of eddies entering the storm track from Asia. Fig 5 (upper panel) shows the histogram of the monthly mean climatological variance of meridional velocity perturbations at 200mb from the 16 years of the NCEP-NCAR Reanalysis (every 6 hours) data set. The variance has been averaged over different sectors of the Pacific storm track. The two curves show the averaged variance for the area of the mid-eastern Pacific storm track (solid line) and the averaged variance for an area characteristic of the storm track entrance in the western Pacific (dashed line). The lower panel shows the ratio of the averaged variance at the entrance over the averaged variance in the eastern region (the two curves in the upper panel). What the upper panel shows is that the seasonal cycle of variability of the storm track intensity has maxima occurring in Fall and Spring. The relative minimum observed in the winter months is the mid-winter suppression discussed by Nakamura (1992). The dashed curve shows the amount of variance at the storm track entrance (upstream seeding). The variance at the entrance also shows a minimum in the winter months. The ratio of the monthly variance between both regions shown in the lower panel can be interpreted as the ratio between downstream development and baroclinic development. If the ratio is close to unity, it means that the same amount of eddy energy at the entrance has been distributed along the storm track

without the contribution of sources and sinks. However for small values, it means that local sources inside the domain are producing further development and increase the eddy energy above the entrance level. It should be concluded from the Figure that:

a) In winter months storm track eddies benefit from downstream development (~40%) and baroclinic sources, whereas in summer months no baroclinic development is present.
b) Moreover, it shows also that because the ratio is more or less constant from October- March, the mid-winter suppression is related to less eddy activity from Asia (or upstream seeding) as suggested by Orlanski (1998).

Fig 6 shows the interannual variability of the January mean variance of meridional velocity perturbations from the NCEP-NCAR Reanalysis. The meridional velocity is the deviation of each January mean at 300mb and the variance is averaged over two regions: for the mid eastern Pacific Ocean (full line) and for a small region (10^o x 10^o) at roughly the entrance of the Pacific storm track (dashed line). The occurrence of the ENSO cycle is also indicated here, el Nino (red) and la Nina (blue). The interannual variability in the Pacific storm track, as well as the seeding upstream could be as much as 50%. The relation between seeding and storm track activity does not show a clear relationship as seen in Fig 5. However, it seems that there is a relation between the eddy activity (high), the seeding (low) and the cold phase of ENSO (N3-). There appears to be some weak relation between el Nino (N3+) and the upstream seeding. For instance, the intensity of the variance is above the mean. The few ENSO cycles of this series is not conducive to a

conclusive cause and effect relation between upstream seeding the SST boundary forcing and the activity of the storm track. It does however point to the fact that there is large interannual variability in both the upstream seeding and the storm track and also to the existence of a relation of upstream seeding and eddy activity for the climatological state (Fig 5). Sensitivity experiments were performed with various seedings in order to understand or at least determine the dependence of eddy kinetic energy along the storm track on the amount of eddy seeding at the entrance. The time evolution of the seeding for two different amplitudes is shown in Fig 7. Moderate seeding has an STD of 4.08m/s and the strong seeding is close to double that, 7.93m/s. Fig 4 shows the eddy kinetic energy for moderate seeding (middle panel) and stronger seeding (lower panel); the strong seeding tends to produce more intense mid storm track eddies.

Eddies reaching intense baroclinicity in the western Pacific Ocean will grow faster to equilibration (closer to the entrance of the storm track) for more intense seeding. As discussed in Chang and Orlanski (1993**),** baroclinic eddies in a storm track environment grew through baroclinicity and downstream development. This means that eddies feel the influence of surface baroclinicity which enhances their intensity and produces stronger energy fluxes downstream to a new growing system. The initial amplitude is larger and the required zonal distance where eddies will mature is shorter**.** Fig 8 displays the Hovmoller diagrams for pressure deviations at z=5500m height, Moderate seeding (left panel) and Strong seeding (right panel). Let us highlight a few important features from these responses. First, the amplitude seems to grow downstream. Second, a prevalent

high at the entrance (red center at 150E) is correlated with a stronger low in the center (blue center at 180) and an even stronger high at the eastern Pacific (red center at 120W). Third, both simulations clearly indicate that the signal from the left is correlated a few days later with the disturbance on the right. Finally, stronger upstream highs are associated with stronger downstream highs for the stronger seeding compared with the moderate seeding. This raises some interesting questions: first, why is there an apparent strong asymmetry between highs and lows for the upstream disturbances? The seeding meridional velocity, a sine function of time, is quite symmetric in Fig 7; a mean meridional circulation is also present. It should be noted that, in normal years (NON-EL NINO) there is a considerable amount of moist fluxes from the subtropics to the extra-tropics (lower right panel Fig 3) over the western Pacific Ocean. As the poleward meridional flow is enhanced, more intense fluxes reach the baroclinic eddies (computed but not shown) and a more intense circulation is generated in comparison with the phase in which the meridional flow is diminished by the equatorward phase of the seeding. This enhances the asymmetry between the anticyclonic and cyclonic circulation at the entrance of the storm track. The second question; what relation exists between a stronger upstream high anomaly in the western Pacific and the response over the PNA sector? Fig 9 illustrates the time-lag regression of meridional velocity (at z=5500m) with the time-series of meridional velocity (shown in Fig 7) at the storm track entrance. A clear signal of downstream development can be seen in both panels of Fig 9. From the slope of the centers we can infer that the group velocity is about 40m/s and the slope of equal phase

(phase velocity) is about 12m/s. Both velocities closely correspond; the group velocity to the upper level flow and the phase velocity to the steering velocity at around 4000m height; the ratio of the velocities is about Cg/Cph=3.3. The upper level response due to the jet baroclinicity and speed has a zonal wavelength close to 56º longitude (4760km, global "m" between 6 and 7) and does not seem to be very sensitive to small variations of the jet conditions. A simple geometric relation shows that with a velocity ratio of 3.3, a high center *H* located in the vicinity of the storm track entrance, (~140 E, pressure centers at t=0, shown by gray circles in the upper panel) will maximize the high response at a distance of roughly 3.3xλ/2 from the initial high, or at around 130W (140E+3.3x56º/2). It seems clear from Fig 9 that the larger the meridional flow is at the entrance, the larger its effect will be downstream. This result is crucial to understanding how natural variability (here as high frequency wave activity entering the storm track region) could drastically change the response in the PNA sector.

b. upper level wave-breaking:

As the waves develop downstream they go though a scale transformation. The second half of the storm track has less baroclinicity and even if the waves grow larger because of upstream fluxes, they become more upper level barotropic with enhanced horizontal scales (Simmons and Hoskins 1979, Orlanski and Chang 1993). This scale expansion can be seen in the time mean upper level pressure anomalies of Fig 3 (upper right panel) and the mid-level pressure disturbances in the Hovmoller diagram of Fig 8. For moderate and

strong seeding, the upper level waves will complete their life-cycle and break as they propagate east. The more intense the baroclinic waves are, the more intense the wave-breaking is and, as shown by Orlanski (2003), the axis of the storm track will be deflected further poleward further enhancing the *H* over the PNA sector. Orlanski (2003) also showed that if the eddy energy is very intense, a bifurcation in the life-cycle can occur and waves instead of breaking anticyclonically could break cyclonically pushing the axis and the jet more equatorward. The level of energy in which the shift is possible is strongly dependent on the horizontal scale of the waves. There is currently no reliable statistical measure of counting the number of waves that break one way or another. A superficial estimate of the energy level for the control solution shows that the level is not sufficient for these wavelengths for the bifurcation to occur. Orlanski (2003) estimates (his Fig 18) that a wavenumber m= 7 should reach at least 400 $(m/s)^2$ and m=6 more than 500 $(m/s)^2$ for the bifurcation to occur. Both solutions with moderate and strong seeding fall short of these threshold energies. Before concluding this section we should clarify the role of seeding in the PNA sector. We have shown that more intense seeding at the entrance of the storm track leads to a more intense poleward deflection of the jet and the axis of the storm track in the eastern region. But a valid question is: what will happen if no seeding or very small seeding is introduced in the western Pacific? We have performed that simulation with a very small seeding (0.1 the amplitude of the moderate seeding) and the results are slightly different from the moderate seeding. Remember that with or without seeding, the entrance of the storm track is baroclinically unstable and

regardless of the initial forced perturbations, eddies eventually will be generated. The initial disturbance produced by the seeding helps increase the eddy development to a finite amplitude closer to the entrance region. However, the north Pacific storm track is not absolutely unstable and requires some seeding. Regardless of the level of the seeding that we impose, there is a constant background seeding from perturbations that recycle from the western subtropical convective region as well as disturbances entering from the western high latitudes to the storm track region. This is why baroclinic eddies are not as dependent on the shape and frequency of the seeding as they are on the amplitude exceeding a critical level (approximately the value used for our moderate seeding). Now that we have a better understanding of the response to normal SST conditions and the variability to external seeding, we can analyze the conditions for tropical SST anomalies.

5. Sensitivity to tropical SSTs:

a**) Mean anomaly conditions due to changes in tropical SST.**

The format of this section will be similar to Section 4. Basically**,** we will introduce a temperature anomaly to the SST shown in Fig 2 for the control experiment (as a convention the control experiment used hereafter is the moderate seeding case previously discussed). We will show two experiments with modified SSTs**.** Exp N1 is a moderate EL NINO case and Exp N2 is a strong EL NINO case. Both experiments use the same seeding as the Control case. The SST anomalies from the Control are shown in Fig 10.

We see an enhanced temperature in the eastern ocean which is confined to the tropical region only. A maximum anomaly of 7^{o}C is specified for the strong El Nino case. Since our approach has been to determine the level of high frequency eddy activity and its feedback to the quasi-permanent flow, it is important to show that not only the so-called PNA can be reproduced but the amplitude as well. For that purpose we show the observed anomalies from the NCEP-NCAR Reanalysis as provided by CDC in Fig 11. The anomalies shown are JAN of EL NINO year conditions minus climatology (1968-1996); in the upper left panel the deviations of the 200mb mean zonal wind are shown; note the deviation of the jet equatorward. The 200mb heights with its characteristic PNA pattern are shown in the upper right panel. The lower panels display the surface air temperature (lower left) and the precipitable water column (lower right). Consistent with the equatorial temperature shift to the east, the precipitable water also has been displaced to the east. A rather similar pattern is shown for the simulations. Since Exp N1 and Exp N2 have very similar responses and Exp N1 is weaker than Exp N2, we will show only one of the solutions , the stronger one corresponding to Exp N2 (strong EL NINO). Fig 12 contains fields similar to those in Fig 11. However, instead of height anomalies, here we show the pressure anomalies; instead of surface air temperature, here we show surface potential temperature anomalies. The similarity with the observed anomalies from the previous figure is striking. The zonal flow, with the same scale (Interval 2m/s), shows a very similar displacement to the tropics. The PNA pattern again has strong similarities;

the minimum pressure anomaly in the simulation is about 8 hPa or about 184m (at 300hPa, 23m/hPA) for Exp N1 is 6hPA and the observed anomaly is about 120m in Fig 11. Although it is more difficult to make a direct quantitative comparison with the other two fields, the overall patterns seem quite satisfactory. This is particularly noticeable for the negative precipitable water in the western tropics and the strong positive anomaly east of the dateline. However, the simulations show a stronger amount of precipitable water anomaly in the western subtropics not shown in the observations. This is perhaps due to an unrealistic warm pool in the western subtropics for the idealized SST used.

b) Anomalies in wave-activity:

The eddy kinetic energy anomaly for Exp N1 and Exp N2 is shown in Fig 13. Both show a distinct displacement of the storm track equatorward with an anomaly amplitude equal to-15 to 20% of the total eddy kinetic energy. The kinetic energy anomaly in both experiments seems to be very similar. However, it is also apparent that values for Exp N1 seem larger than Exp N2. This issue will be discussed later in this section. Let us now analyze the effect of tropical SSTs on the extra-tropical pressure disturbance. The large anomaly in the western subtropic shown in Fig 13 is a product of, a not very significant but persistent convective activity for the ENSO warm phase simulations, perhaps due to the idealized SST used in the simulations and western boundary condition. However, these disturbances did not seem to affect or interact with the storm track. Fig 14, similar to Fig 8, shows the Hovmoller diagram of the pressure deviation from zonally averaged

initial conditions for the Control, Exp N1 and Exp N2 (Note that the meridional extent of the averaging is sufficiently large to encompass any meridional displacement expected for the storm track). Two distinct differences in the pressure response are immediately apparent between N1, N2 and the Control. Although the seeding amplitude is the same in the three solutions, Control has a slightly larger amplitude at the entrance of the storm track and a much larger amplitude at the exit. On the other hand, N2 with the stronger tropical SST has the weakest amplitude. Furthermore, the trough in the middle storm track seems consistently more intense for the stronger EL NINO case N2. It seems evident that the high frequency eddies have a considerable influence on the enhancement or weakness of the quasi-permanent disturbance in the eastern Pacific Ocean. It is clear that downstream development from the western ocean is present in most cases with different degrees of intensity. Additionally, Exps N1 and N2 having more or less the same intensities in the western Pacific Ocean, there is a consistently weaker intensity of the ridge over the PNA sector for the stronger SST anomaly case. Consequently, we may conclude that baroclinic eddies are probably primarily responsible for the sensitivity of the storm track to tropical SSTs. We will investigate how sources and sinks for those eddies can change due to changes in the tropical circulation.

c) Sources and Sinks:

The heat flux vector anomaly (minus control) and its divergence for the lower layers (z=1300m) are shown for both N1 and N2 in Fig 15. This figure shows that both N1 and

N2 have more poleward heat fluxes than Control on the equator side of the storm track. This result suggests that more baroclinicity should be extended equatorward for the El NINO cases. A number of studies have examined the eddy energy budgets of baroclinic waves (e.g. Smith 1969, Kung 1977, Orlanski and Katzfey 1991 among others) Employing the form and interpretation of the budget suggested by Orlanski and Katzfey (1991) yields a budget of the form

$$\frac{\partial E}{\partial t} = -\nabla \cdot \overline{\langle vE + v'_a p' \rangle} - \frac{g(\overline{v'\theta'} \cdot \nabla\Theta)}{\Theta_m \langle \frac{\partial \Theta}{\partial z} \rangle} - \overline{v' \cdot \langle v' \cdot \nabla \rangle V_m} - diss + diab$$

where the bar indicates the time average for the period; the prime indicates the deviation of that average and <> indicates a large area and time average. The first term on the RHS is the energy and pressure fluxes, the second term is the baroclinic conversion, the third term is the barotropic conversion and the last two terms are the dissipation and diabatic effects. Note that the convention used for baroclinic and barotropic conversion has a positive tendency for the eddy energy when either one is negative.

The baroclinic conversion anomaly for N1 and N2 is shown in Fig 16 for two levels z=1300m and z= 5500m. For N1 and N2 the salient characteristic is more baroclinic conversion on the equator-side of the eastern storm track. The contours show the variance of the eddy potential temperature anomaly which is consistent with the eddy kinetic energy anomaly (Fig 13). Both experiments have larger values on the southern side. From

Fig 15 and Fig 16 we can conclude that baroclinic conversion is being displaced equatorward. The upper level barotropic conversion anomaly in Fig 17 also exhibits the same feature. It seems that the Control has a more intense barotropic conversion on the poleward-side than either El Nino experiments. To summarize the predominant eddy sources and sinks, Fig 18 displays the pressure fluxes and baroclinic conversion for the Control (upper panel, N1 (middle panel) and N2 (lower panel). The inclined rectangle is for reference only. The dark purple area indicates very strong baroclinic conversion to the eddies**;** the white region within the purple area for both N1 and N2 shows that the maximum exceeds the selected scale (5×10^{-4} m/s^{o}K^{2}/m). This figure suggests that both N1 and N2 have an intensified baroclinic conversion over the mid-Pacific region and stronger pressure fluxes over the southeastern ocean and the west coast of North America. N1 and N2 appear to have a more intense source of baroclinicity over the subtropical eastern part of the Pacific Ocean.

d) Baroclinic Sources:

Fig 19 shows the potential temperature anomaly for El Nino years from the NCEP-NCAR Reanalysis at 500mb in the upper panel; the lower panel displays the potential temperature anomaly for N2 at z=5500m (N1, having a very similar pattern, is not shown). We show this level because as Fig 16 showed, the baroclinic conversion extends deep into the atmosphere. In spite of the quantitative differences**,** there is a remarkable

qualitative similarity between the idealized simulations and the observed anomalies. We have shown that both the observed and simulated cases have increased baroclinicity around 30N, a region associated with the maximum divergence of heat fluxes (Fig 15). It seems that at least in the simulations the warm region is related to the equatorial convective region and SST anomalies are being displaced eastward. A zonally averaged (from 180 to 140W) cross section of the potential temperature, liquid water and meridional wind vector anomalies are shown in Fig 20 for N2. There is a large temperature anomaly over the entire subtropical region with a very deep baroclinic zone in the middle latitudes which is consistent with the previous figure. The warm anomalies seem very well correlated with the liquid water anomaly (proxy for latent heat) and also are consistent with the poleward meridional circulation of the Hadley circulation. The cold anomaly in the upper tropical and subtropical atmosphere is related to the lifting of the tropopause due to more intense convection. The Reanalysis displays a similar pattern (not shown here).

e) SSTs and natural variability.

The conclusions for the effects of wave seeding in the western Pacific Ocean (Sec 4) clearly show that the stronger the waves are coming into the storm track, the sooner they reach equilibration amplitude and due to downstream development, the more intense the upper level disturbances are that reach the eastern Pacific coast. On the other hand, the

movement of the equatorial SSTs to the east (EL NINO conditions) produces a more intense baroclinic zone in the middle of the Pacific storm track and as a consequence, stronger cyclonic developments occur south of the climatological (Control) storm track. The cyclonic development due to the enhanced baroclinicity in the eastern part of the storm track seems to compete with the eddies entering from Eastern Asia reducing the amplitude of the ridge over the PNA sector. Moreover, there is a different scale selectivity for both mechanisms**.** The baroclinic eddies that develop from the seeding of eastern Asia feed on the baroclinicity at the entrance of the storm track and tend to expand on the zonal scale due to the downstream development process and become more barotropic, due to the fact that the low level baroclinicity for these cases is rather weak in the middle to the eastern Pacific basin**.** The baroclinic waves are fluxing energy downstream predominantly in the upper levels, and since they do not have a strong low level source, they become upper level barotropic waves with expanded zonal scales. To the contrary, for cases in which the SST anomalies are to the east (EL NINO years), the baroclinicity in the subtropics of the mid-to-eastern Pacific Ocean is enhanced considerably and the eddies that develop or redevelop in these regions will remain with a shorter scale more characteristic of cyclone waves. Fig 21 illustrates these scale differences very well. It shows the pressure anomaly regression for extreme experiments**.** The Control(S) (with strong seeding)**,** discussed in the previous section, is shown in the upper panel and the strong SST anomaly case (Exp N2) is shown in the lower panel.

Since the short time span of the experiments, 70 days, does not allow us to filter the disturbances with high and low pass frequencies, instead we performed a regression of the pressure using the meridional velocity at one longitude (marked with the X) as a proxy of the high frequency response (Chang 1998). For reference, the time mean pressure deviations from the initial zonal averaged pressure at that level is shown with shading. Fig 21 probably should be considered the most important result of the study. It reveals a few facts we have discussed that are central to the issues of understanding the variability of the storm tracks. *a*) The size of the time mean pressure deviations in the PNA sector have roughly the same size as the regressed transient waves and *b*) that the zonal scales of the disturbances are considerably different for the Control (S) (arrow = 2955km, global wavenumber m ~6.8) and the SST(N2) (arrow = 2333km, m ~8.6) simulations. From *a* and *b* we have two major conclusions: the time mean anomalies are being produced by the feedback of the transient eddies and that western Pacific sources produce longer waves over the eastern Pacific than for the case in which the source of baroclinicity is moved to the mid-ocean. We will continue this discussion in the next section.

These two competing mechanisms gave a strong variability to the response of the ENSO cycle. To prove this conjecture we have run a simulation with the same SST conditions of Exp N1 but with strong seeding as described for the Control case in sec 4.(see Fig 7). Fig

22 shows the Hovmoller diagram for the Control (M) (moderate seeding, left panel), Exp N1 (moderate seeding, middle panel from hereafter "N1 (M)") and the new simulation Exp N1 (strong seeding from here after "N1(S)", right panel). Fig 22 has two fields, Control (M) and Exp N1 (M) as in Fig 14, whereas the third graph represents the new simulation. Note that in Fig 22 the anomalies with respect to the mean of Control(M) for the three solutions are shown. These solutions are qualitatively quite similar. It is clear that the pressure height anomaly in the western Pacific for N1(S) is consistently stronger than either the Control (M) or N1 (M). As a consequence of the stronger seeding**,** it seems that the height over the eastern PNA sector for N1(S) is stronger than N1 (M)**.** To corroborate this result the pressure anomaly at the upper levels (z=8900 m) for Exp N1 (M) (upper panel) and Exp N1(S) (lower panel) are shown in Fig 23. Although there is a qualitative resemblance between both responses, it is clear that the strong seeding has weakened the anomaly considerably (about 70%). The SST anomaly pushes the subtropical jet, baroclinicity and storm track equatorward whereas the stronger seeding at the entrance of the storm track due to the downstream development produces upper level barotropic waves in the eastern Pacific with predominantly anticyclonic wave breaking and poleward momentum fluxes.

6. Summary and Conclusions

The work presented is quite distinct from the many articles written on the subject. First, a

high resolution nonhydrostatic cloud resolving model is used to simulate the Pacific storm track and its sensitivity to tropical SSTs and natural variability. The experiments are designed to treat the upstream seeding and the effect of tropical SST anomalies independently. This article has three goals to assess: first, how much the natural variability, measured as high frequency waves entering the western Pacific storm track, can affect the response over the eastern sector; second, how tropical anomalous SSTs can produce the well known response over the PNA region; and finally, how the natural variability interferes with the surface boundary forcing to provide a great variability in the storm track response on the PNA region. The discussion on the effect of storm track seeding by waves entering from the Asian continent first focuses on the normal years. Section 4 shows that two mechanisms operate to distribute the eddy energy along the storm track: downstream development and baroclinic development. The large effect on baroclinic development at the storm track entrance is due to a combination of different factors, surface baroclinicity, land-sea contrast and strong moist fluxes from the western subtropics. The large longitudinal gradients of baroclinicity, with its maximum at the storm track entrance, is due to the fact that as eddies grow from the entrance and along the storm track; they mix the ocean SST and thus reduce the baroclinicity along it. Moreover, waves entering the storm track from the cold continent receive a considerable amount of surface heat fluxes that energizes them, and the fact that a large amount of moisture exists in normal years on the western subtropics is an extra source for wave growth. This explain the sensitivity to the seeding amplitude in our experiments, Control

(M) vs. Control (S), is so large. The larger the seeding amplitude is, the closer the more intense baroclinic waves and intense wave-breaking are to the entrance. As shown by Orlanski (2003), the axis of the storm track will be deflected further poleward thus further enhancing the *ridge* over the PNA sector. A superficial estimate of the energy level for the Control solution shows that bifurcation probably will not occur because the energy level is less than the threshold level for these wavelengths.

The sensitivity to SST anomalies shows qualitative and quantitative similarity with the observed anomalies. The upper level zonal wind pressure patterns and eddy kinetic energy show a very similar displacement to the tropics. Tropical surface air temperatures and column liquid water are displaced eastward during the observed warm phases of ENSO. The experiments show that the PNA pattern is enhanced for a stronger SST anomaly (Exp N2 respect of Exp N1). Those cases also identify the existence of a secondary source of baroclinic development in the middle of the storm track (dateline). This was shown by Orlanski (1998) for a small number of observed ENSO cycles. Further investigation relates the increased baroclinicity in the mid-Pacific to the fact that stronger convection in the mid-tropical Pacific enhances a large pool of warm air over the entire mid-eastern subtropical ocean. This pool of warm air is the source of enhanced baroclinicity in the region. This eastward displacement of the baroclinic zone in EL NINO years produces an extra source for baroclinic development in the mid-eastern Pacific Ocean. These baroclinic waves tend to reduce the effects over the PNA region of

the waves originating at the entrance of the storm track. However, the waves with sources at the storm track entrance break anticyclonically and produce the ridge in the eastern Pacific. The baroclinic waves generated or regenerated in the middle of the ocean tend to break cyclonically and produce a trough tendency, by then reducing the amplitude of the eastern ridge. The two main effects that play an important role in the maintenance of the quasi-permanent circulation are the downstream development from the storm track entrance and the displaced baroclinicity in the middle of the ocean for EL NINO conditions. We use Exp N1(S), a simulation with strong seeding and an SST anomaly similar to N1(M), to prove that conclusion. This shows that increasing the amount of seeding decreases the equatorward displacement of the storm track axis, basically reducing the feedback of the SST anomalies.

These results strongly suggest that: a) the variability of the quasi-permanent circulation could indeed be produced by the high frequency eddy feedback. b) Two main mechanisms operate for the forcing of the quasi-permanent circulation; *downstream development* from the western ocean and the anomalous *baroclinicity in the mid-eastern Pacific.* The intensity of these two counteracting forcings gives different flavors of the El Nino response over the PNA region. It should be noted that regardless of weak and strong SST anomalies, the PNA patterns seem unique but obviously have different intensities. Fig 24 presents a summary of these mechanisms controlling the response over the eastern Pacific Ocean for normal and enhanced tropical SSTs as just discussed. Although we did not specifically show cases with negative SST anomalies (La Nina conditions), it follows

that a cold anomaly in the eastern tropical ocean will further reduce the possibility of baroclinic development at these longitudes and enhance the effect of the building ridge in the PNA sector. These results suggest that perhaps combining methods that account for both the SST anomaly and the amount of eddy activity at the entrance of the storm track could improve significantly our ability to better predict the interannual response over the PNA sector.

Appendix

The model.

Zetac[2] is a fully compressible nonhydrostatic atmospheric model developed at GFDL for regional weather and climate simulations. It uses a hierarchy of time steps (for acoustic-gravity waves, advection, physical parameterizations and radiative forcing) in order to provide solutions for a wide variety of phenomena, from global(see Orlanski and Kerr 2004) to cloud-resolving. It is now coupled, within the GFDL Flexible Modeling System, to component models of the ocean, land and cryosphere. Zetac uses a C-grid in terrain-following coordinates. All the runs done for this study use open boundary conditions at the west (120E) and east (85W). The model used is a stand alone (no ocean or land model coupling). We ran the model without radiative forcing or land/ocean modl coupling, choosing instead to impose a reference wind and temperature profile through nudging at the western boundary. For this study we chose the simplest of microphysical packages, namley a Kessler scheme. Although the resolution could be variable, the simulation uses a 1/4.25 (4/17) degree horizontal resolution to achieve reasonable detail and affordable computer performance. However, for testing the convergences of our solutions to higher horizontal resolutions, we have used a 1/8.5 (2/17) degree horizontal grid. A snapshot of both solutions for a particular simulation is shown in Fig A1. The vertical integrated cloud water after running 10 days is shown for both resolutions. The first thing to notice is the great detail of the clouds and mesoscale structure that the 1/8.5

2 Model developed by Steve Garner (see www.noaa.gov/~stg#zetac)

resolution exhibits. The overall large scale cloud patterns are quite similar. The similarity extends not only to the extratropical systems that seem to be controlled by the synoptic phenomena, but, also to the deep tropical systems (see the south west corner). These results are consistent with new simulations[3] for the tropical atmosphere with the ZETAC model and cloud-resolving scales. Recent experiments for 2km, 4km 8km horizontal resolutions tend to show that the probability distribution function of vertical velocity is quite different in the tails, with the 2km resolution reaching the highest velocities. However, the rest of the distribution seems very similar for all the different resolutions.

3Personal communication from Olivier M. Pauluis

Acknowledgments: I would like to thank Isaac Held for the useful comments that helped clarify the manuscript and to Tom Knutson for the thorough review of the paper. I am grateful to Steve Garner for his efforts in developing the ZETAC model used in this study. Finally I would also like to thank Larry Polinsky for editing the manuscript and to Remik Ziemlinski for creating the display for the snapshots shown in the Appendix, to Chris Kerr for providing valuable programing support and to the GFDL Operations Staff that so efficiently scheduled the experiment runs.

Figures

Fig 1. Cross section of the zonal jet, potential temperature and water vapor forced at the entrance of the storm track in the western Pacific Ocean.

Fig 2. Sea surface temperature used for the Control simulation. It shows larger meridional temperature gradients and higher equatorial temperatures in the western region, similar to the climatological state (contour interval=4^{o}C).

Fig 3. The 50 day time averaged fields for the Control solution (moderate seeding). Zonal wind at the upper levels (CI=10m/s, upper left). Pressure deviation of the zonally averaged initial pressure (CI=2hPa, upper right). Surface Potential temperature (CI=4^{o}C, lower left) and surface water vapor (CI=0.002g/Kg, lower right).

Fig 4. Variance of the transient meridional velocity for the NCEP-NCAR Reanalysis and two Control simulations. January 300mb variance of the meridional velocity from NCEP-NCAR reanalysis (upper). The model simulations are at z=8900m, the "Control (M)" with moderate seeding (middle panel) and with strong seeding "Control (S)" (lower panel) the contour interval for all the panels is 50m^{2}/s^{2}.

Fig 5. Area average of variance of the meridional velocity at the two locations of the storm track (upper panel) mid-eastern region (full line) and the entrance region (dashed

line). The ratio of the entrance region over the mid region variance is shown in the lower panel (see text).

Fig 6. The January variance for meridional velocity, area averaged (170E:130W and 30N:50N, 300mb) representing the Mid-eastern Pacific storm track(full line) and the variance for meridional velocity area averaged (120E:130E and 30N:50N) at the entrance of the storm track. The January means are calculated using the daily data for the 16 year span 1983 to 1998 NCEP-NCAR Reanalysis. The color arrows indicate the occurrence of the major events of the ENSO cycle (see text).

Fig 7. The area average (10^{o}x10^{o}) variance for meridional velocity of the two control simulations forced with moderate seeding and strong seeding. The forced seeding, although random in amplitude and frequency, are the same but the strong seeding has double the amplitude of the moderate seeding.

Fig 8. Hovmoller diagram of the pressure deviations for Control (M) left panel and Control (S) right panel; the contour interval is 2.5hPa for both panels.

Fig 9. Time-lag regression of the meridional velocity at z=5500m for both simulations Control (M) upper panel and Control (S) lower panel. The regression is done using the time history of the meridional velocity averaged 10^{o}x10^{o} degrees at z=5500m. The labels

H and L in the upper panel indicate the position of the pressure deviation extrema at 0 time-lag.

Fig 10. SST anomaly from experiments N1**,** moderate equatorial SST (upper panel) and N2**,** strong equatorial SST (lower panel). In both panels the contour interval is 1°C.

Fig 11. The January CDC composite anomaly fields for El Nino years using El Nino 3.4 time series (NCEP-NCAR Reanalysis data). The zonal wind anomaly at 200mb (upper left panel), the 200mb height anomaly is shown in the upper right panel. The surface air temperature (lower left) and column precipitable water content are displayed (lower right). The zero contour is the boundary between the white and pink colors.

Fig 12. This figure is similar to Fig 10 but for the simulations. The panels show the anomaly fields between Exp N2 and Control: the zonal wind at 8900m (upper left), the pressure anomaly at z=8900m (upper right), the surface potential temperature anomaly (lower left) and the precipitable water content (lower right). The zero contour is the boundary between the white and pink colors.

Fig 13. The anomaly eddy kinetic energy (z=5500m) is shown for both EL NINO experiments. In the upper panel is the difference between N1 and the Control and in the lower panel for experiment N2 (the units are in m^2/s^2).

Fig 14. The Hovmoller diagram for pressure deviation from the initial conditions for the three experiments: Control (left panel), N1 (center panel) and N2 (right panel); this is similar to Fig 7. Again, blue indicates low pressure and red high pressure (CI=2.5hPa).

Fig 15. Anomalies of the energy flux vector (defined in text) and the divergence of the flux vector (in color) is shown for N1 (upper panel) and for N2 (lower panel).

Fig 16. Anomalies of baroclinic conversion (anomalies of eddy energy tendencies are positive in blue areas) and the variance of potential temperature at two heights: z=1300m (upper panels) and z=5500m (lower panels) for N1 (left panels) and N2 (right panels).

Fig 17. Barotropic conversion (defined in text; eddy energy tendencies are positive in red areas in m^2/s^3) at z=8900m for Control (upper panel) and N2 (lower panel).

Fig 18. Baroclinic conversion (Eddy growth in the purple area) at z=5500m (CI=0.55×10^{-3} and max purple 5.5×10^{-3} m^2/s^3) and Pressure flux vectors at z=8900m for Control (upper panel), N1 (middle panel) and N2 (lower panel). The rectangular frame is for reference.

Fig 19. Time mean potential temperature anomaly for January of El Nino years from NCEP-NCAR Reanalysis (CDC) at z=500mb (upper panel) and N2 – Control at z=

5500m.

Fig 20. Cross-section of the time averaged potential temperature anomaly for N2-Control (color shading) anomaly of liquid water content Qc (blue contour) and meridional vector anomalies (vertical velocities are multiplied by a factor=50). These fields are averaged in over 40^{o} longitude and centered at 160W.

Fig 21. Regression of the upper level pressure (z=8900m, black contours) vs. time series of mid-level meridional velocity (at z=5500m, averaged over 30N:50N at long.=140W. Marked with X) in hashed red and blue (positive and negative areas) is the time mean pressure deviations at z=8900m, for the two extreme cases, Control with strong seeding Control(S) (upper panel) and N2 with the strong SST anomaly (lower panel). The arrows are as reference for ease in detecting the scale of the disturbances**.** The arrow for Control (S) represents a distance of 2955Km, and global wavenumber m~6.8; whereas the arrow for N2 is equal to 2333km with an equivalent m~8.6.

Fig 22. Very similar to Fig 14 showing the Hovmoller diagram for pressure deviation but of the mean Control experiment**:** Control(M) (moderate seeding, left panel), N1(M) (moderate seeding, center panel) and N1(S) (strong seeding, in the right panel). Again, blue indicates low pressure and red high pressure (CI=2.5hPa).

Fig 23. Upper level pressure anomaly for N1(M)-Control(M) (upper panel) and N1(S)-Control(M) (lower panel).

Fig 24. A schematic presentation of the mechanisms that control the atmospheric response along the Pacific storm track, for normal years and El Nino years. The solid arrows indicate the position of the upper level jet; the wavy-lines represent the eddies and indications of the change in horizontal scale for different regions along the storm track. The wavy lines on the extreme left depict the waves entering from Asia, whereas wavy lines on the extreme right indicate the waves that characterize the high frequency response at the end of the storm track. Note that on the subtropical branch of the storm track the waves characteristic lengths are shorter than on the polar branch. The blue areas represent the low-level baroclinicity that shift to the east following the SST anomalies. The dashed-arrows represent the downstream fluxes that are enhanced by the pool of low level baroclinicity. The blue arrow indicates fluxes emanating from the storm track entrance whereas the red arrow shows the enhanced flux due to the shifting of the baroclinic pool eastward.

Fig A1. Shows two snapshots of the Control simulation with two different resolutions, 1/(4.25) degrees and 1/(8.5) degree horizontal resolution. Integrated column liquid water is shown.

References

Chang, E. K. M, Lee, Sukyoung, Swanson, Kyle L. 2002: Storm Track Dynamics. *J. Climate*, **15**, 2163-2183.

_____. 1993: Downstream development of baroclinic waves as inferred from regression analysis. *J. Atmos. Sci.*, **53**, 2850-2875.

_____ and Orlanski, I. 1993. On the Dynamics of a Storm Track. *J. Atmos. Sci.*, **50**, 999-1015.

Geisler, J. E., Blackmon, Maurice L., Bates, Gary T., Muñoz, S. 1985: Sensitivity of January Climate Response to the Magnitude and Position of Equatorial Pacific Sea Surface Temperature Anomalies. *J. Atmos. Sci.*, **42**, 1037-1049.

Held, I. M., Ting, Mingfang, Wang, Hailan. 2002: Northern Winter Stationary Waves: Theory and Modeling. *J. Climate*, **15**, 2125-2144.

_____, Lyons, S. W. and Nigam, S. 1989: Transients and the extratropical response to El Nino. *J. Atmos. Sci.*, **46**, 163-174.

Hoerling, M. P., Kumar, Arun. 2002: Atmospheric Response Patterns Associated with Tropical Forcing. *J. Climate*, **15**, 2184-2203.

Kumar, A., Hoerling, Martin P. 1997: Interpretation and Implications of the Observed Inter-El Niño *J. Climate*, **10**, 83-91.

Kung, E. C. 1977: Energy Sources in Middle-Latitude Synoptic-Scale Disturbances. *J. Atmos. Sci.*, 34, 1352-1365.

Kushnir, Y, Robinson, W. A, Bladé, I, Hall, N. M. J, Peng, S, Sutton, R. 2002: Atmospheric GCM Response to Extratropical SST Anomalies: Synthesis and Evaluation*. *J. Climate*, **15**, 2233-2256.

Lau, N. -C. and Nath, M. J. 1991: Variability of the Baroclinic and Barotropic Transient Eddy Forcing Associated with Monthly Changes in the Midlatitude Storm Tracks. *J. Atmos. Sci.*, **48**, 2589-2613.

Madden, R. A. 1976: Estimates of the Natural Variability of Time-Averaged Sea-Level

Pressure. *Mon. Wea. Rev.*, **104**, 942-952.

Nakamura, H. 1992: Midwinter Suppression of Baroclinic Wave Activity in the Pacific. *J. Atmos. Sci.*, **49**, 1629-1642.

Orlanski, I. 2003: Bifurcation in Eddy Life Cycles: Implications for Storm Track Variability. *J. Atmos. Sci.*, **60**, 993-1023.
_____ 1998: Poleward Deflection of Storm Tracks. *J. Atmos. Sci.*, **55**, 2577-2602.

_____, Chang, Edmund K. M.. 1993: Ageostrophic Geopotential Fluxes in Downstream and Upstream Development of Baroclinic Waves. *J. Atmos. Sci.*, **50**, 212-225.

_____, Katzfey, J. 1991: The Life Cycle of a Cyclone Wave in the Southern Hemisphere. Part I: Eddy Energy Budget. *J. Atmos. Sci.*, **48**, 1972-1998.

Palmer, T.N., Owen, J.A.. 1986: A Possible Relationship between Some "Severe" Winters in North America and Enhanced Convective Activity over the Tropical West Pacific. *Mon. Wea. Rev.*, **114**, 648-651.

Simmons, A.J., Wallace, J.M., Branstator, G.W.. 1983: Barotropic Wave Propagation and Instability, and Atmospheric Teleconnection Patterns. *J. Atmos. Sci.*, **40**, 1363-1392.

_____, Hoskins, Brian J. 1979: The Downstream and Upstream Development of Unstable Baroclinic Waves. *J. Atmos. Sci.*, **36**, 1239-1254.

Smith, R.K.. 1969: On the Effects of Vorticity Entrainment in Zonal Jet Flows. *J. Atmos. Sci.*, **26**, 1233-1237.

Trenberth, K. E. 1993: The different flavors of El Nino. *Proc. 18 Annual Climate*

Dynamics Workshop, Boulder, CO, National Oceanic and Atmospheric Administration,

50-53.

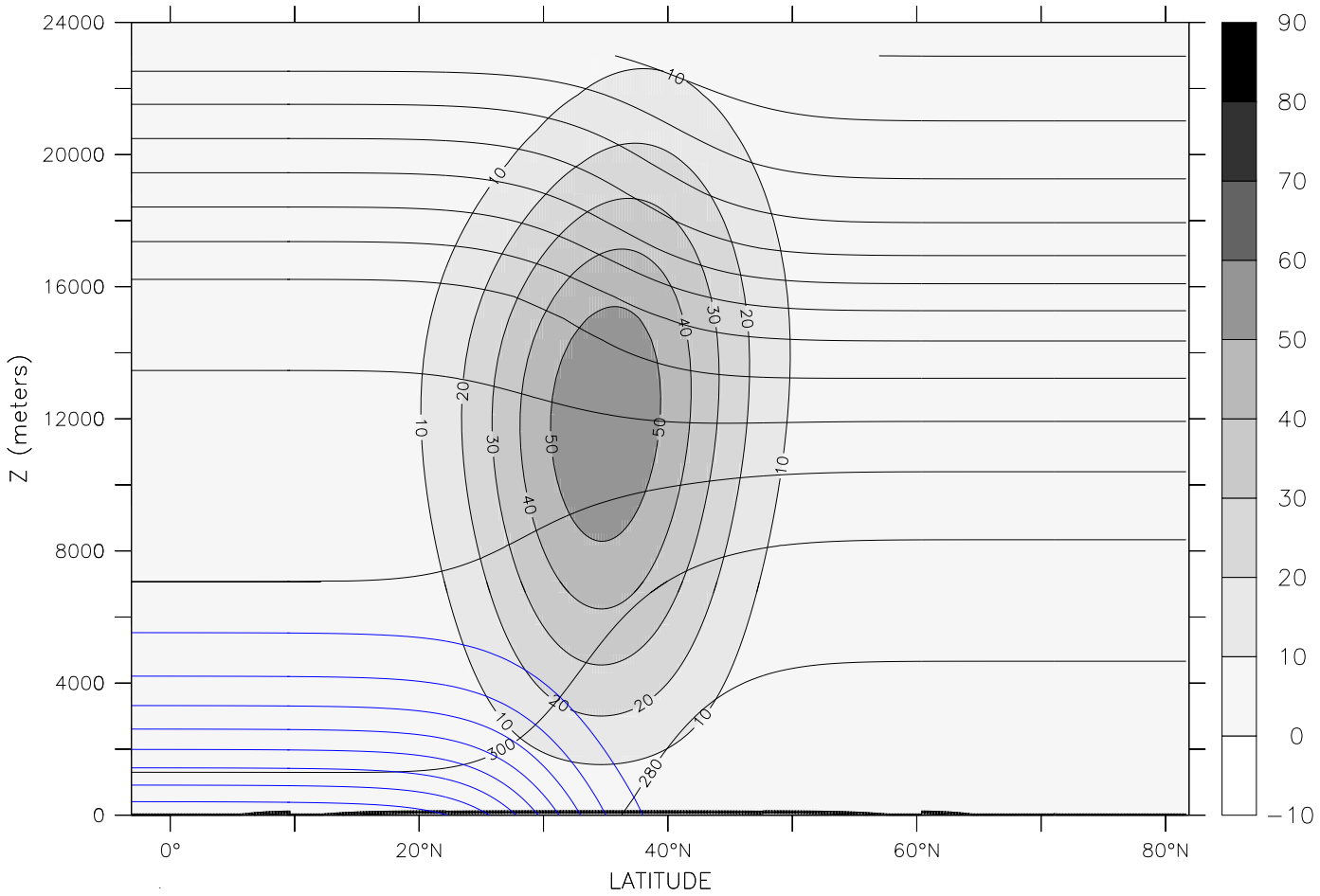
24000
20000
16000
12000
8000
4000
0
Z (meters)
0°
20°N
40°N
60°N
80°N
LATITUDE
90
80
70
60
50
40
30
20
10
0
−10

Fig 1

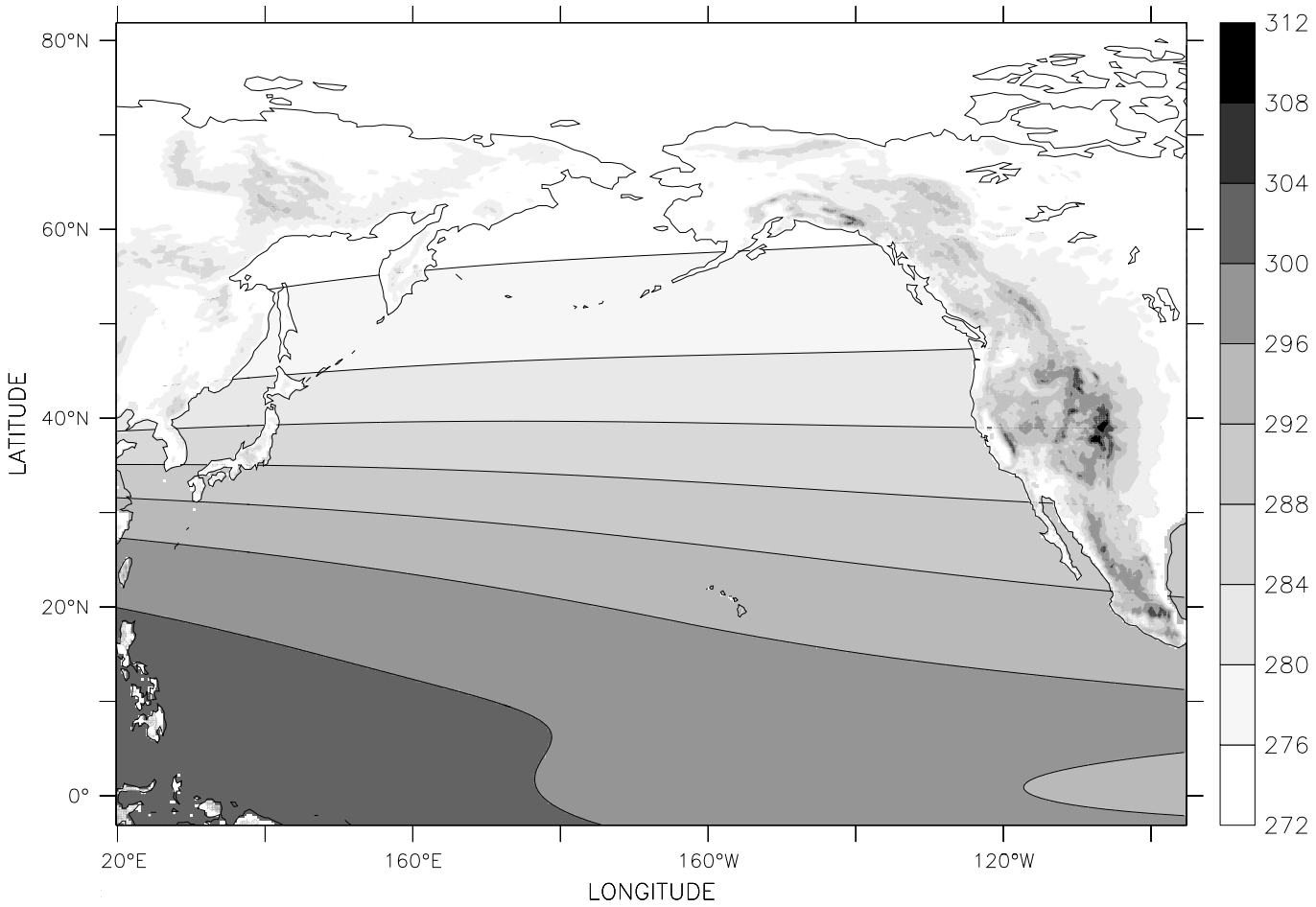
80°N
60°N
40°N
20°N
0°
LATITUDE
20°E
160°E
160°W
120°W
LONGITUDE
312
308
304
300
296
292
288
284
280
276
272

Fig 2

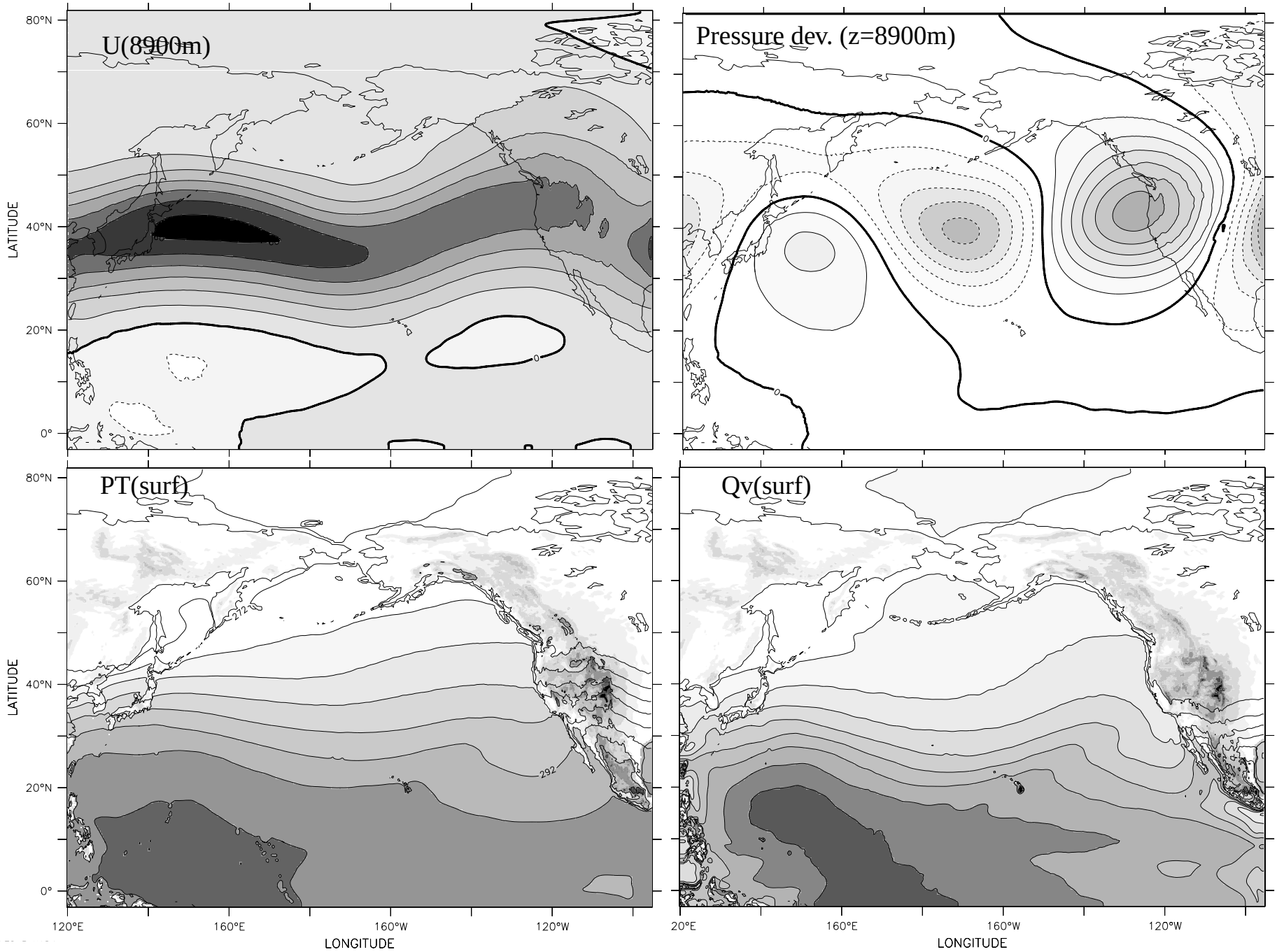
U(8900m)
Pressure dev. (z=8900m)
PT(surf)
Qv(surf)
80°N
60°N
40°N
20°N
0°
LATITUDE
120°E
160°E
160°W
120°W
20°E
LONGITUDE
0
292

Fig 3

Variance of Upper Level Meridional Velocity

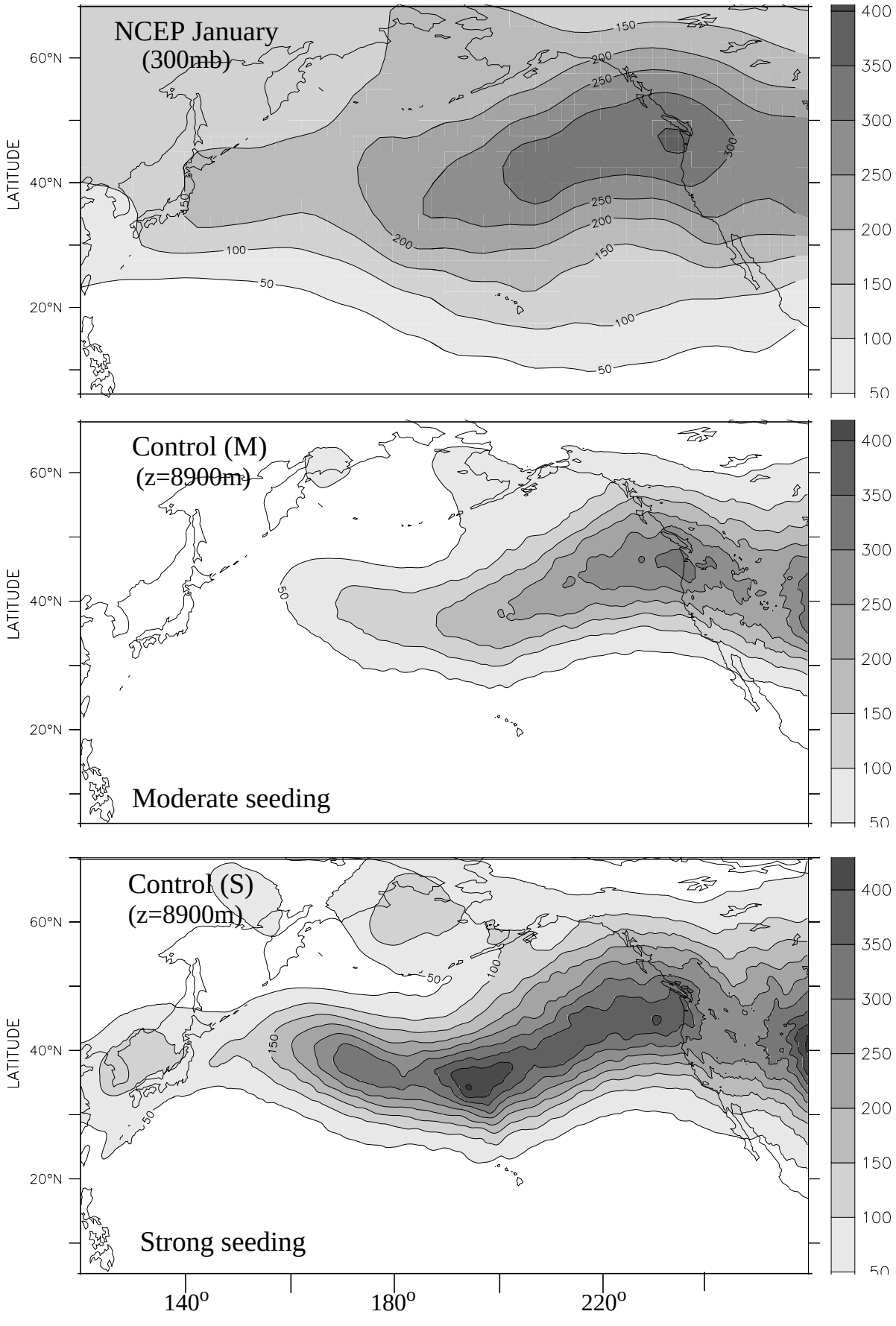

Fig 4

Area Averaged of Variance of Meridional Velocity (200mb) along the Pacific Storm track
the data is meridionally averaged 30N:50N

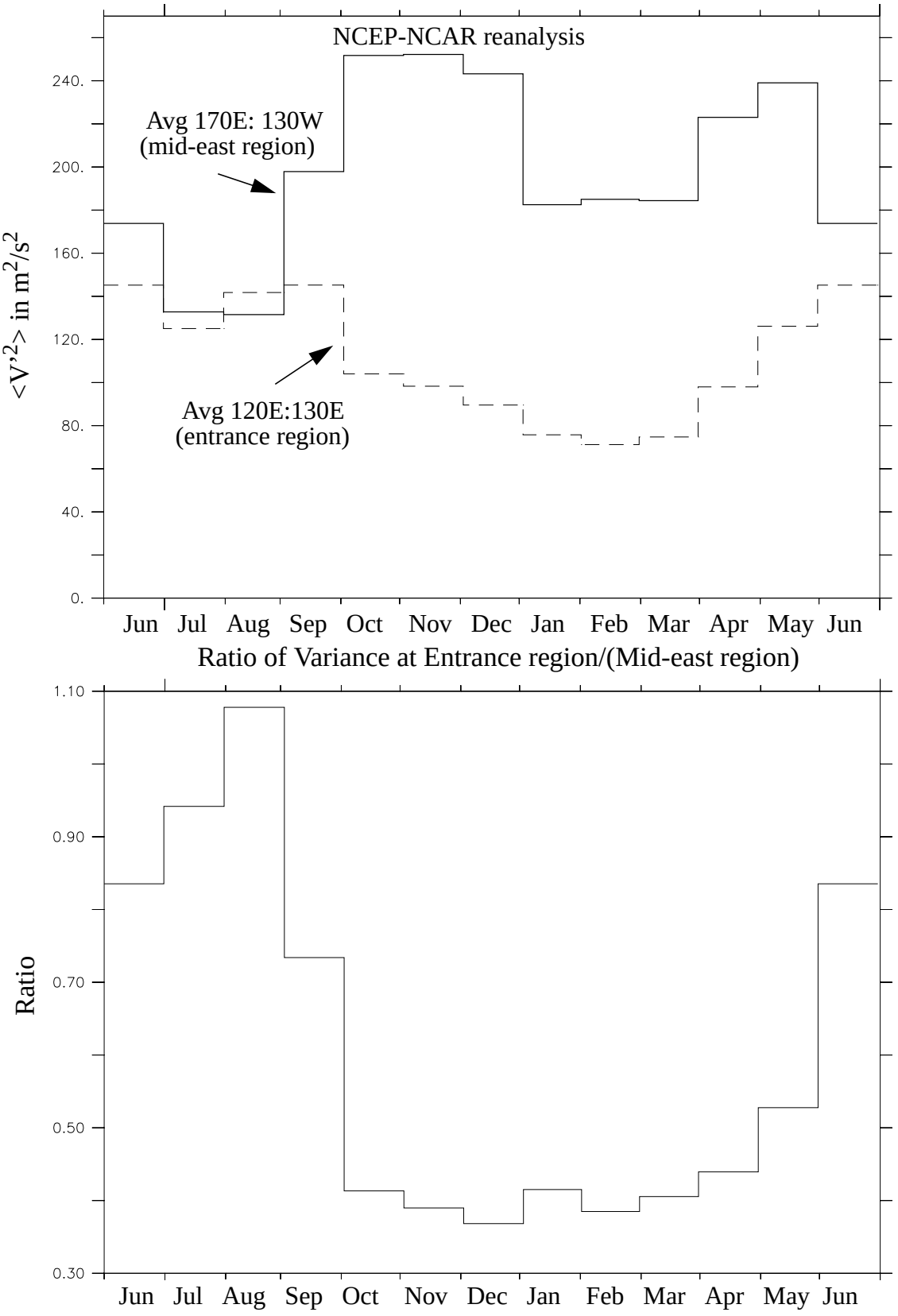

Fig 5

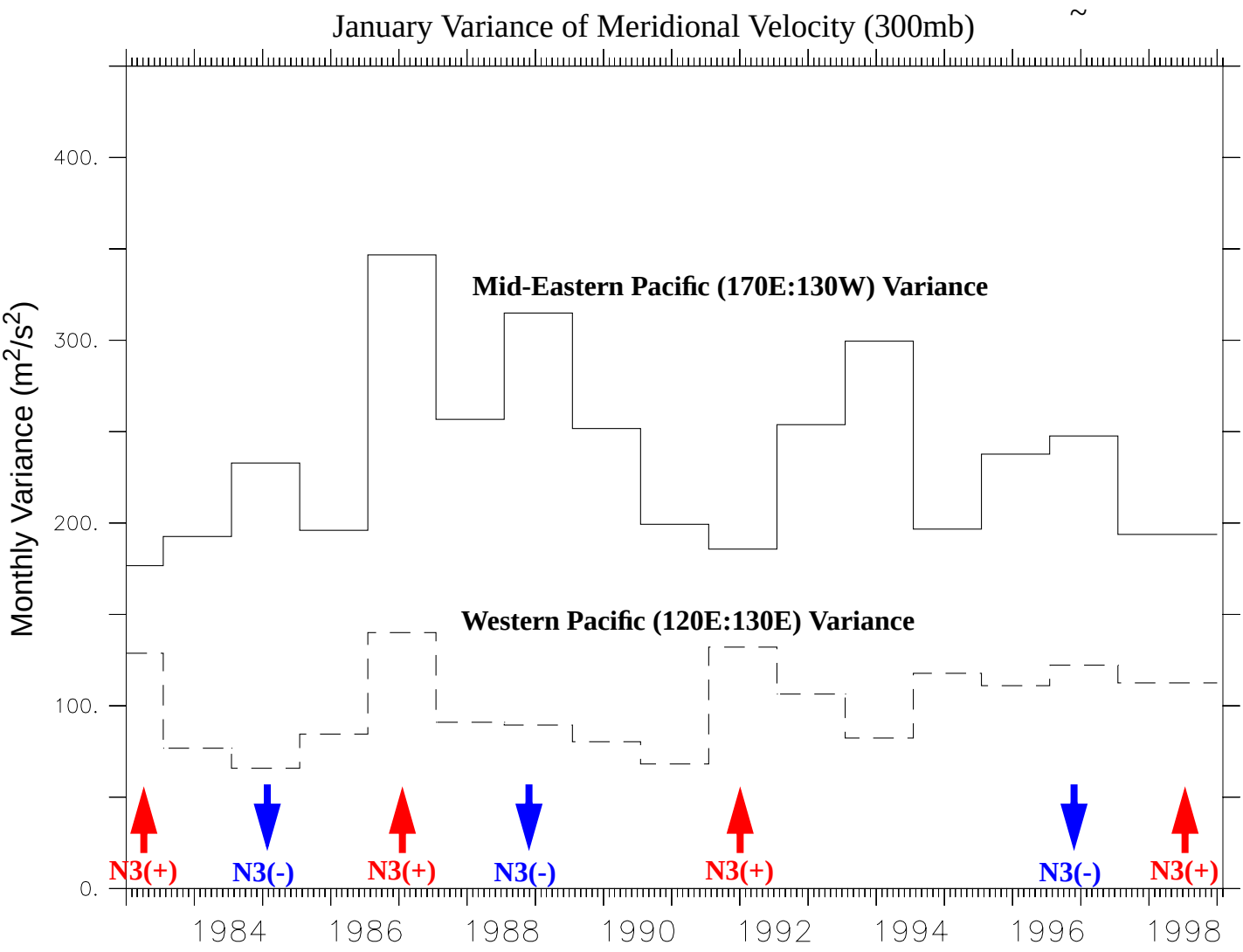
January Variance of Meridional Velocity (300mb)
Monthly Variance (m2/s2)
400.
300.
200.
100.
0.
Mid-Eastern Pacific (170E:130W) Variance
Western Pacific (120E:130E) Variance
N3(+)
N3(-)
N3(+)
N3(-)
N3(+)
N3(-)
N3(+)
1984
1986
1988
1990
1992
1994
1996
1998

Fig 6

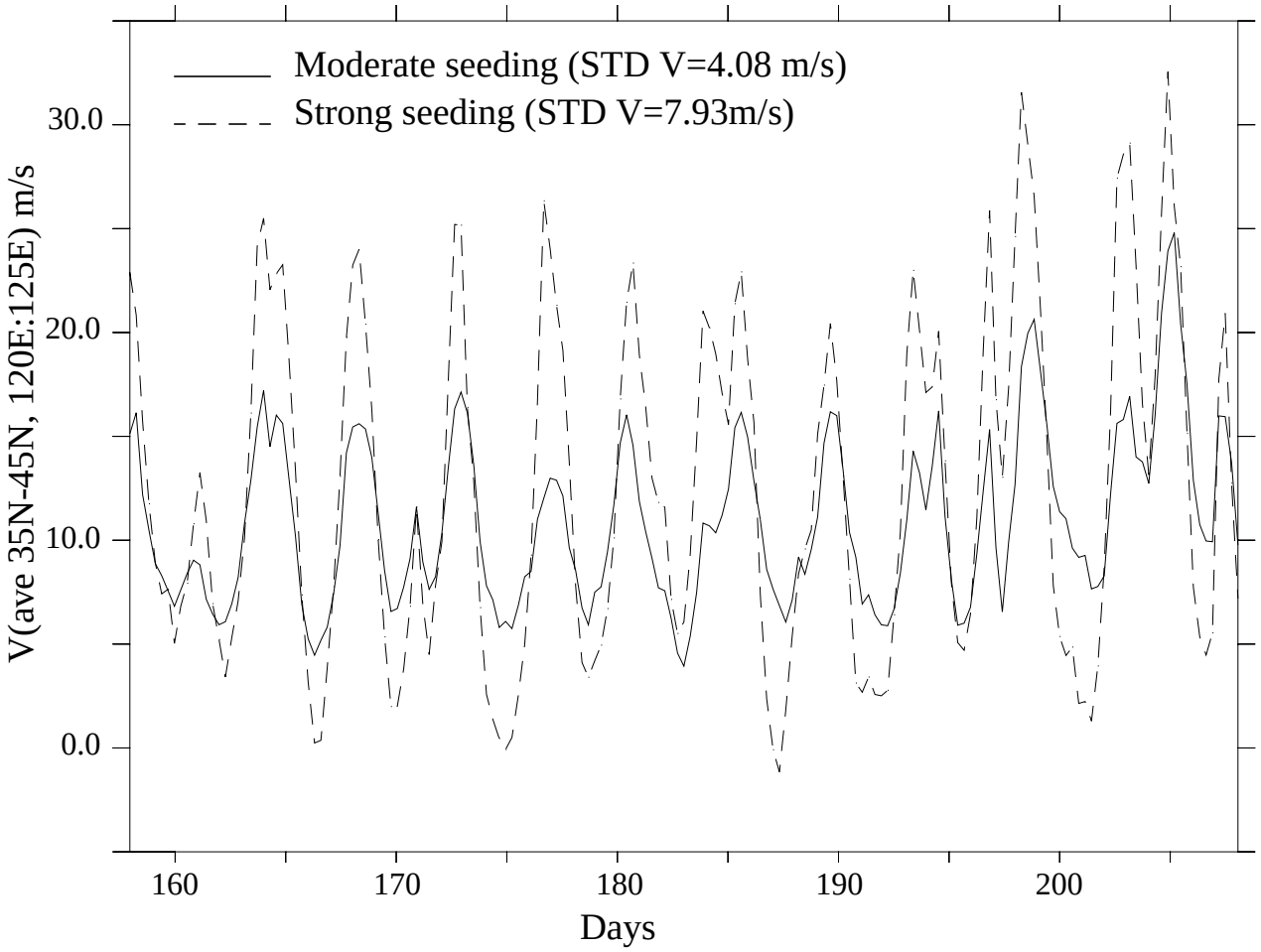
Meridional Velocity (z=8900m/s) at the entrance of the Storm Track
Moderate seeding (STD V=4.08 m/s)
Strong seeding (STD V=7.93m/s)
V(ave 35N-45N, 120E:125E) m/s
30.0
20.0
10.0
0.0
160
170
180
190
200
Days

Fig 7

Hovemoller Diagram of Pressure deviation from Initial (z=5500m)
(30N-50N averaged)

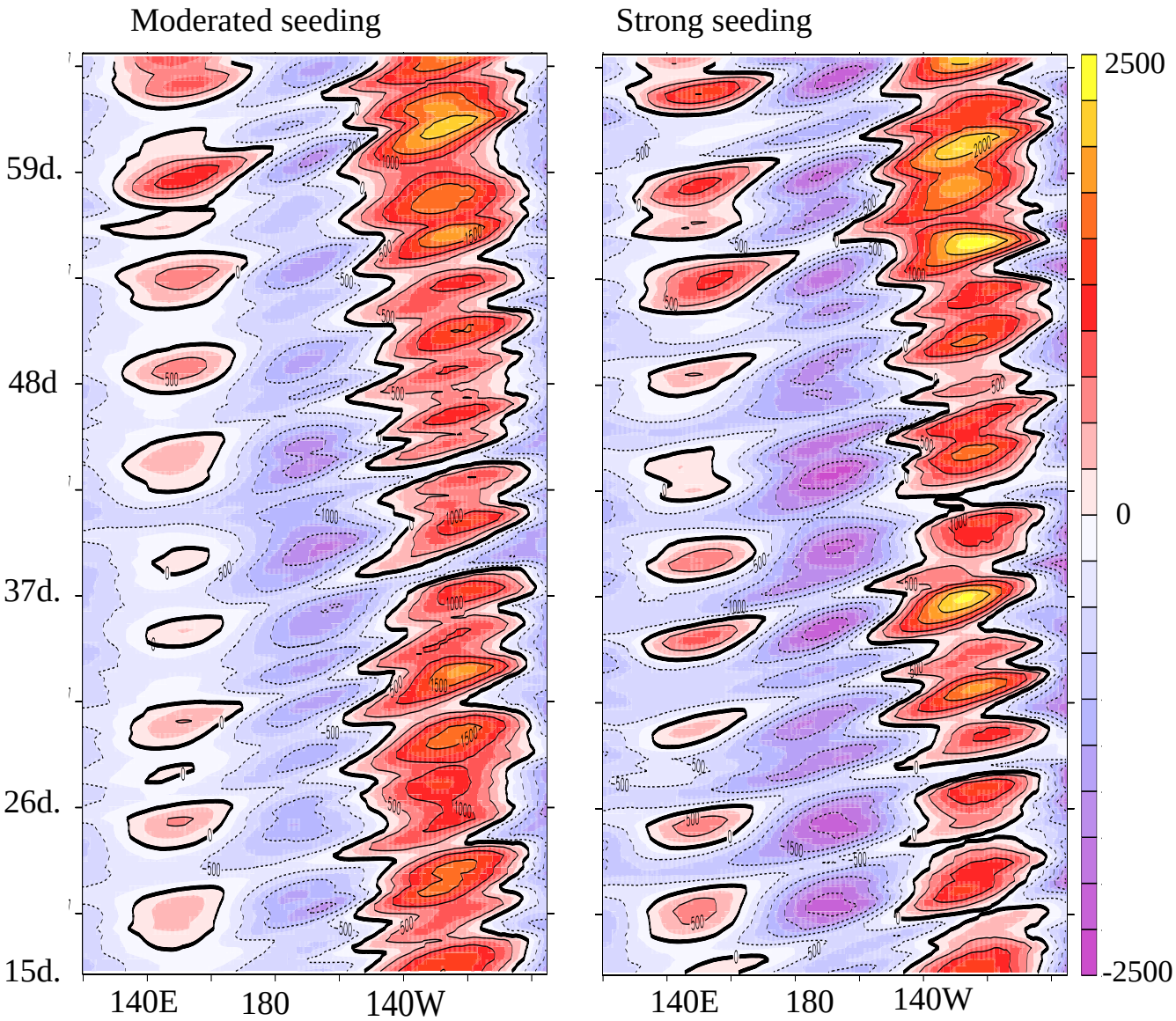

Fig 8

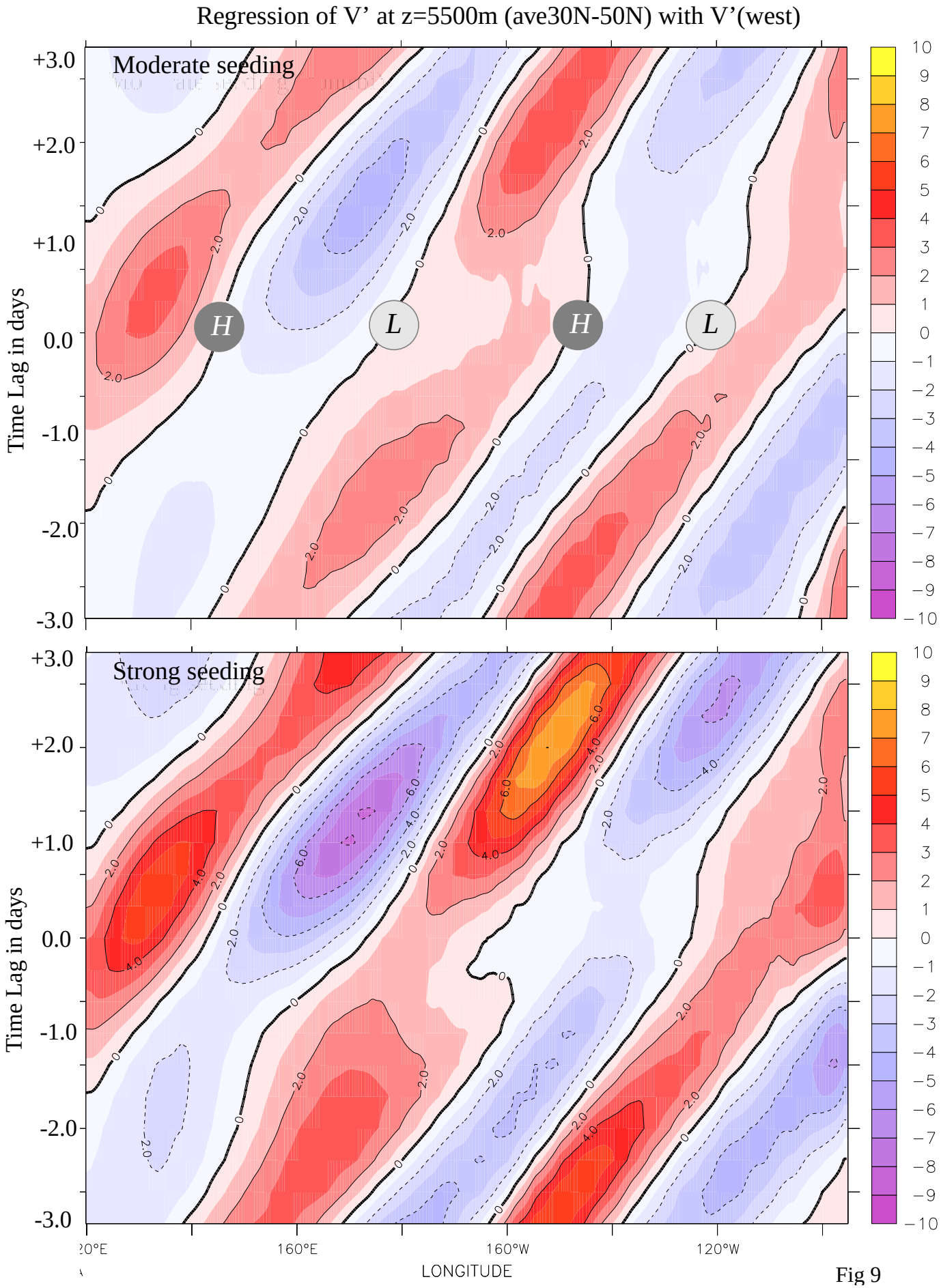
Regression of V' at z=5500m (ave30N-50N) with V'(west)
Moderate seeding
Strong seeding
H
L
H
L
Time Lag in days
+3.0
+2.0
+1.0
0.0
-1.0
-2.0
-3.0
160°E
160°W
120°W
LONGITUDE

Fig 9

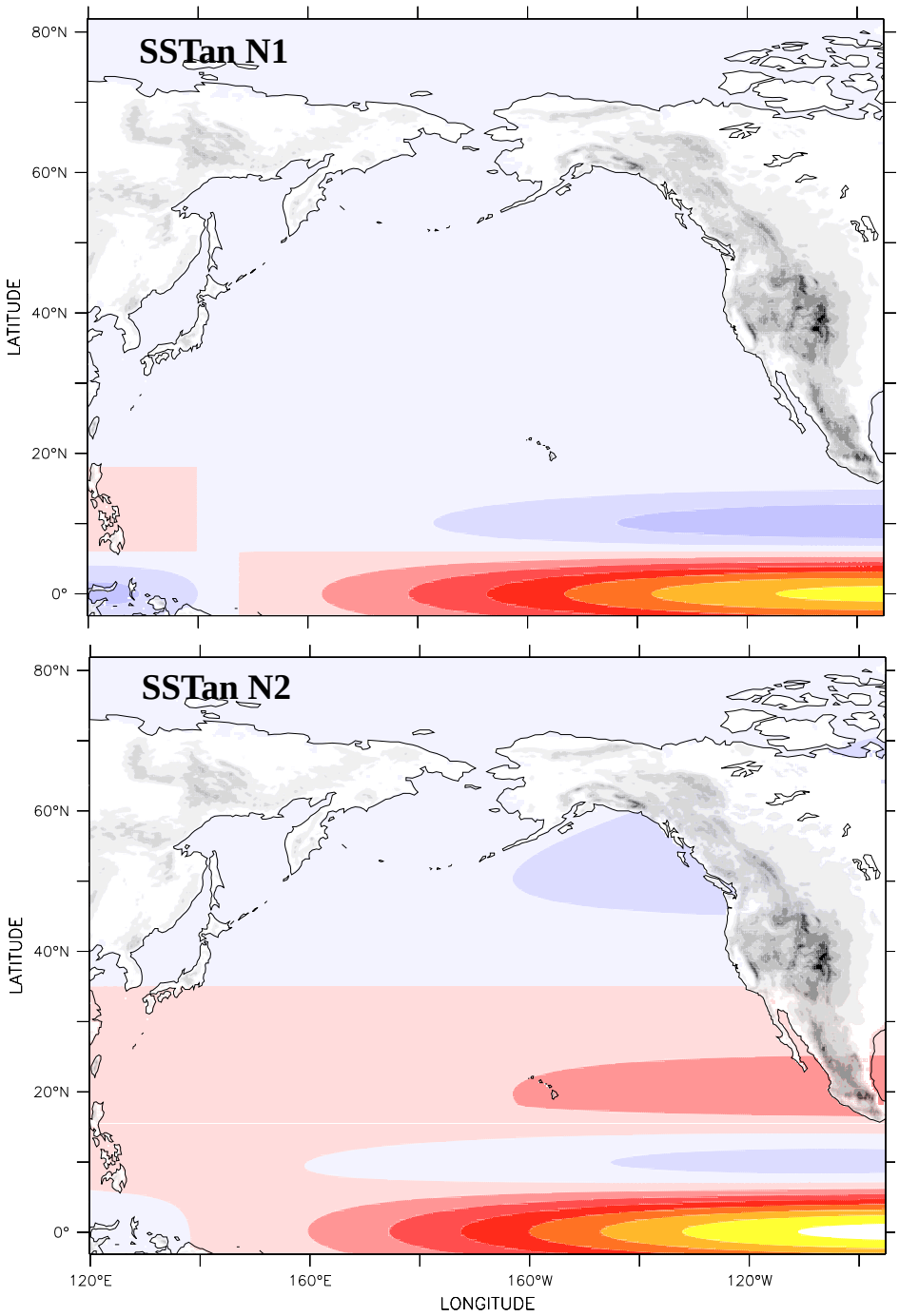
SSTan N1
SSTan N2
80°N
60°N
40°N
20°N
0°
LATITUDE
120°E
160°E
160°W
120°W
LONGITUDE

Fig 10

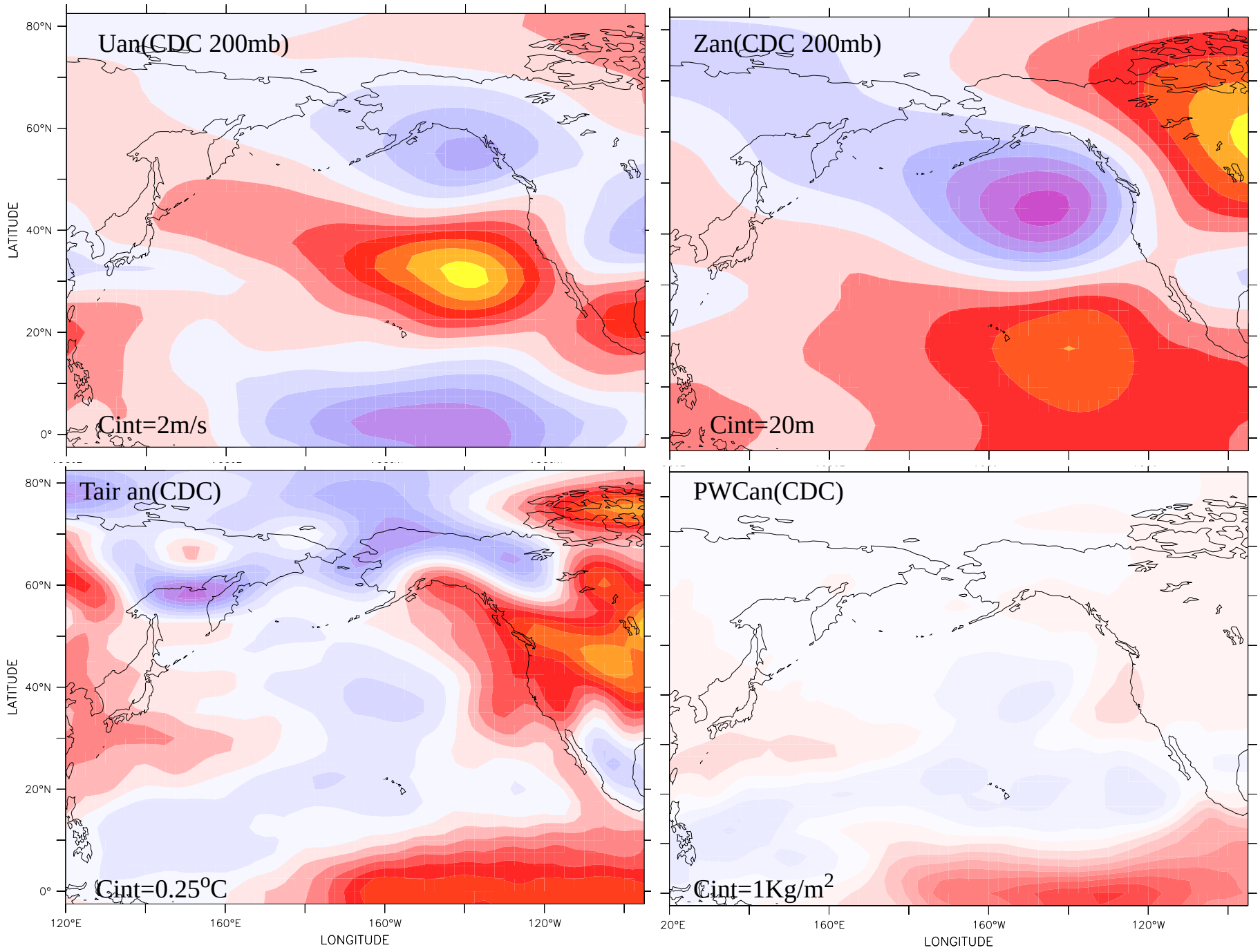
Uan(CDC 200mb)
Cint=2m/s
Zan(CDC 200mb)
Cint=20m
Tair an(CDC)
Cint=0.25°C
PWCan(CDC)
Cint=1Kg/m2
80°N
60°N
40°N
20°N
0°
LATITUDE
120°E
160°E
160°W
120°W
20°E
LONGITUDE

Fig 11

Anomaly Fields for EXP N2

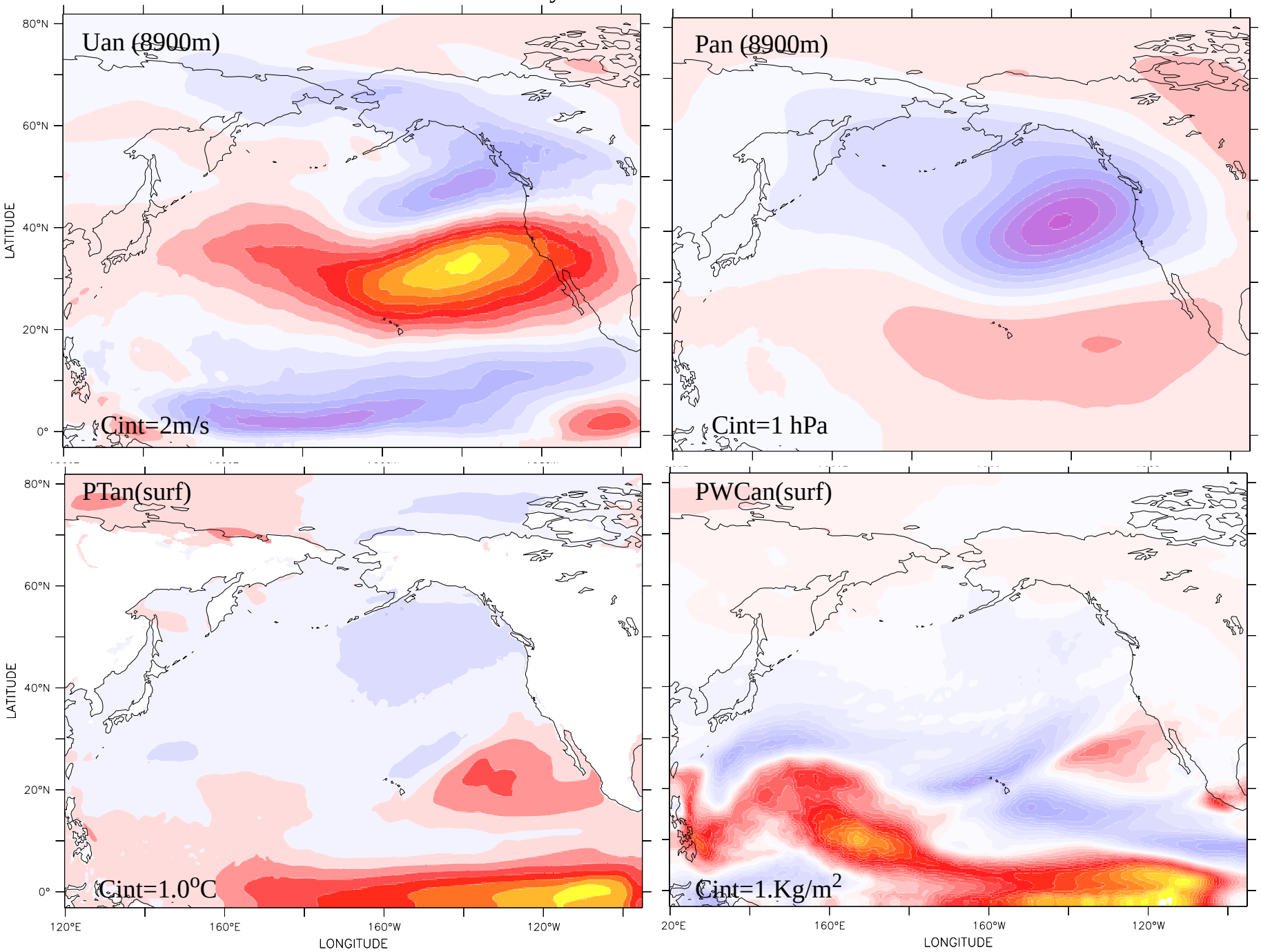

Fig 12

Anomaly Eddy Kinetic Energy (z=5500m)

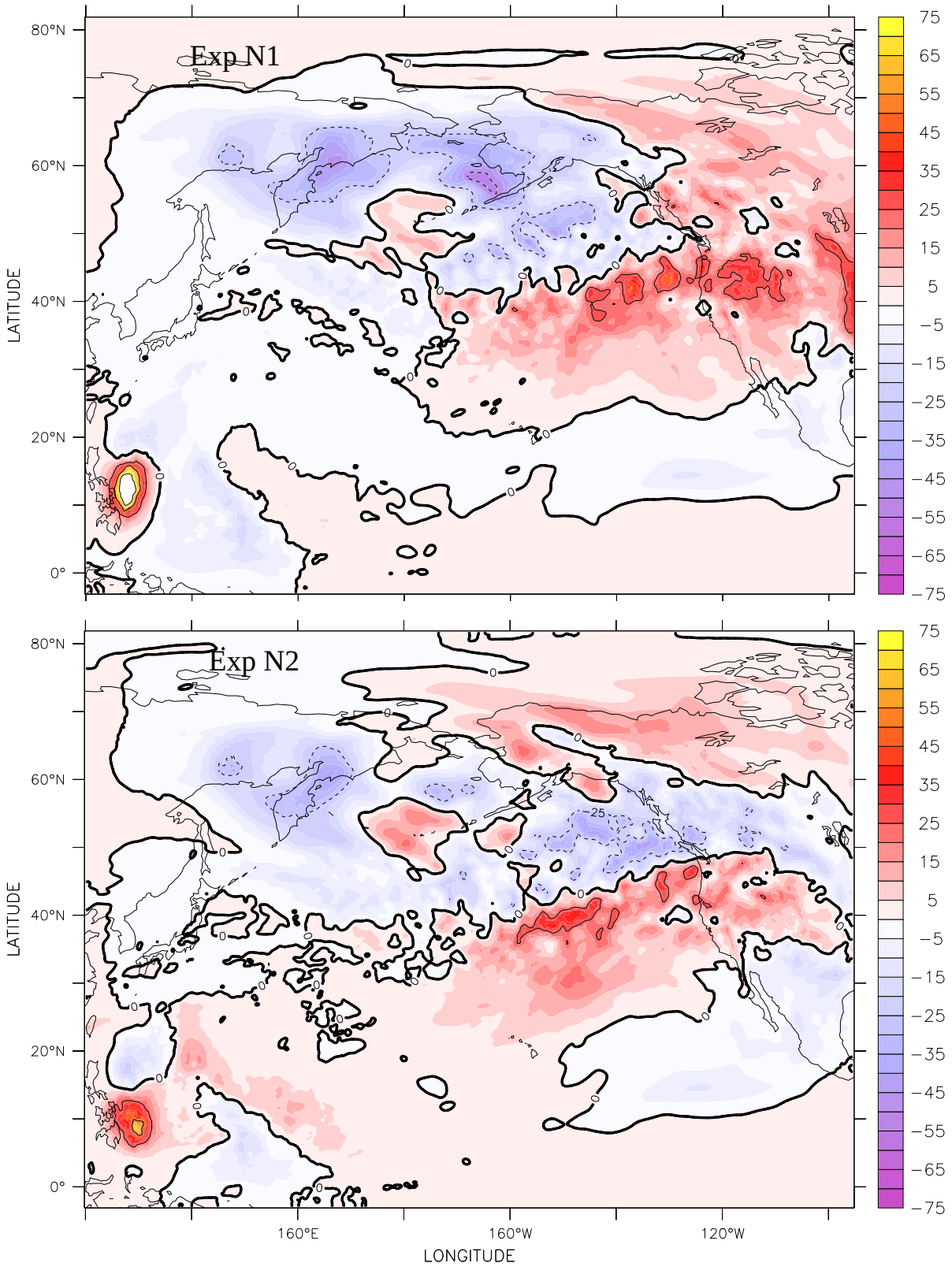

Fig 13

Hovmoller Diagram of Pressure Deviations (z=5500m) of Initial zonal Pressure (averaged 30N,50N)

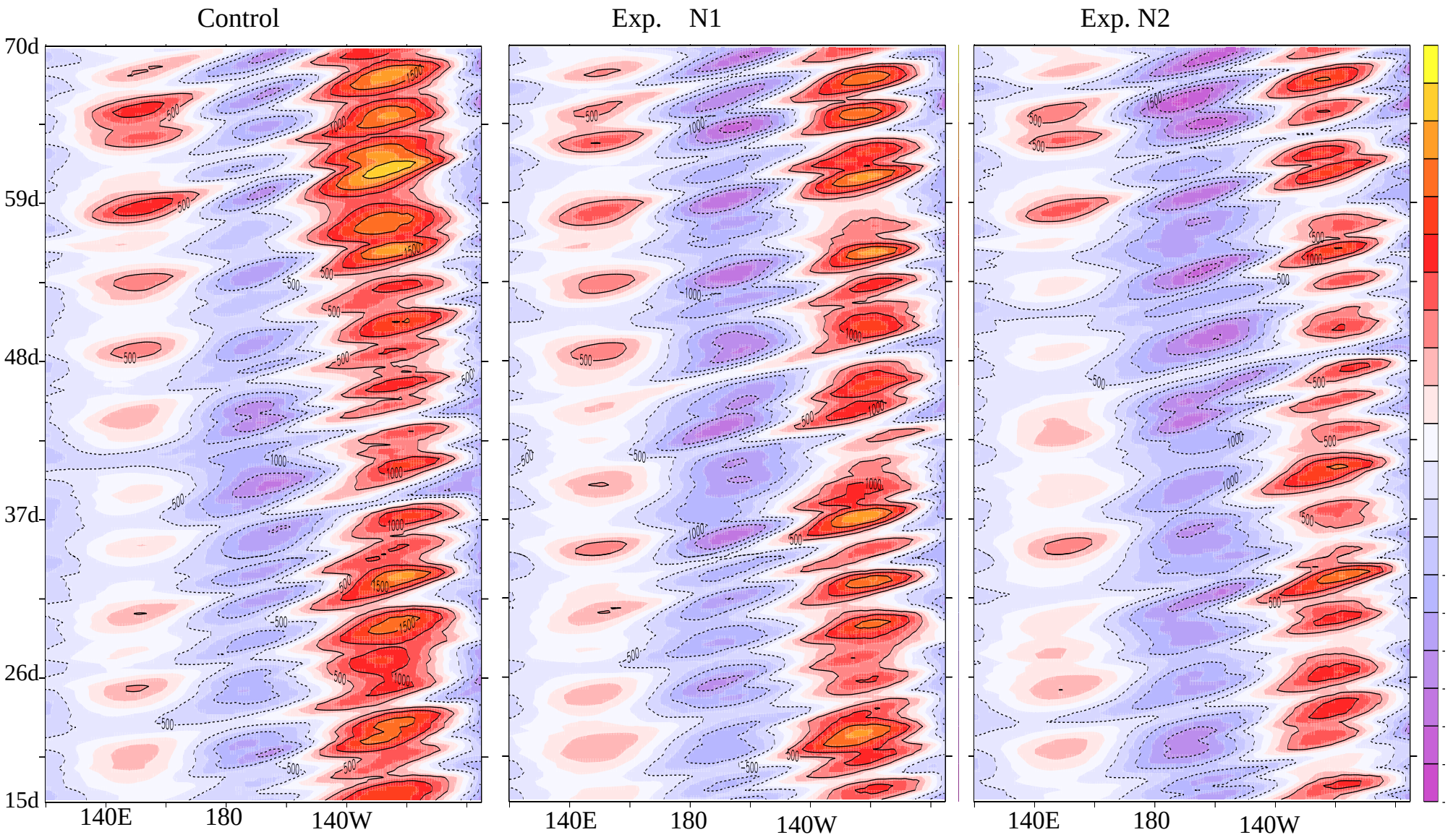

fig 14

Anomaly Heat Flux vector and Divergence (color) (z=1300m)

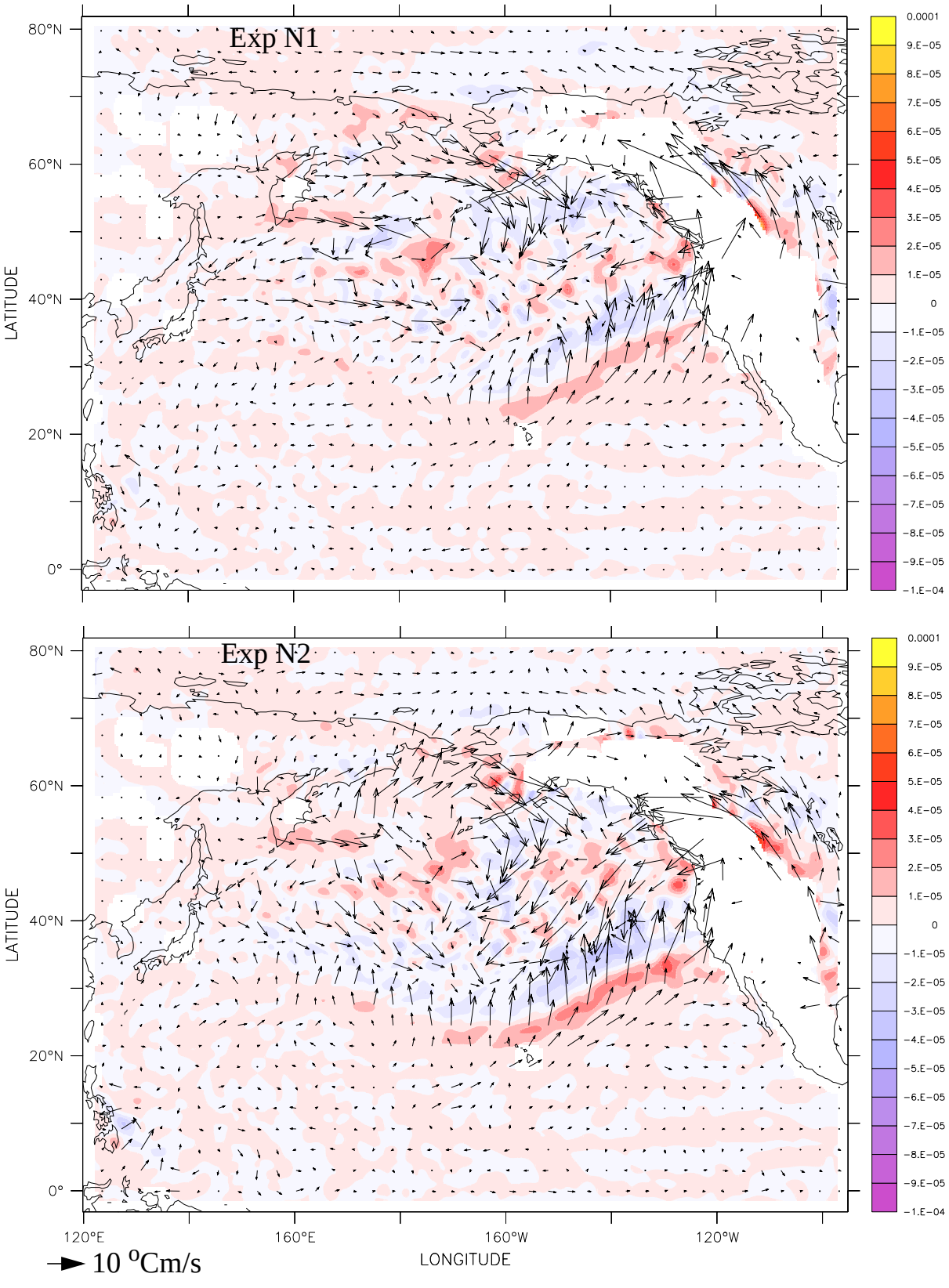

Fig 15

Baroclinic Conversion (color) Anomaly Variance of Potential temperature (black)

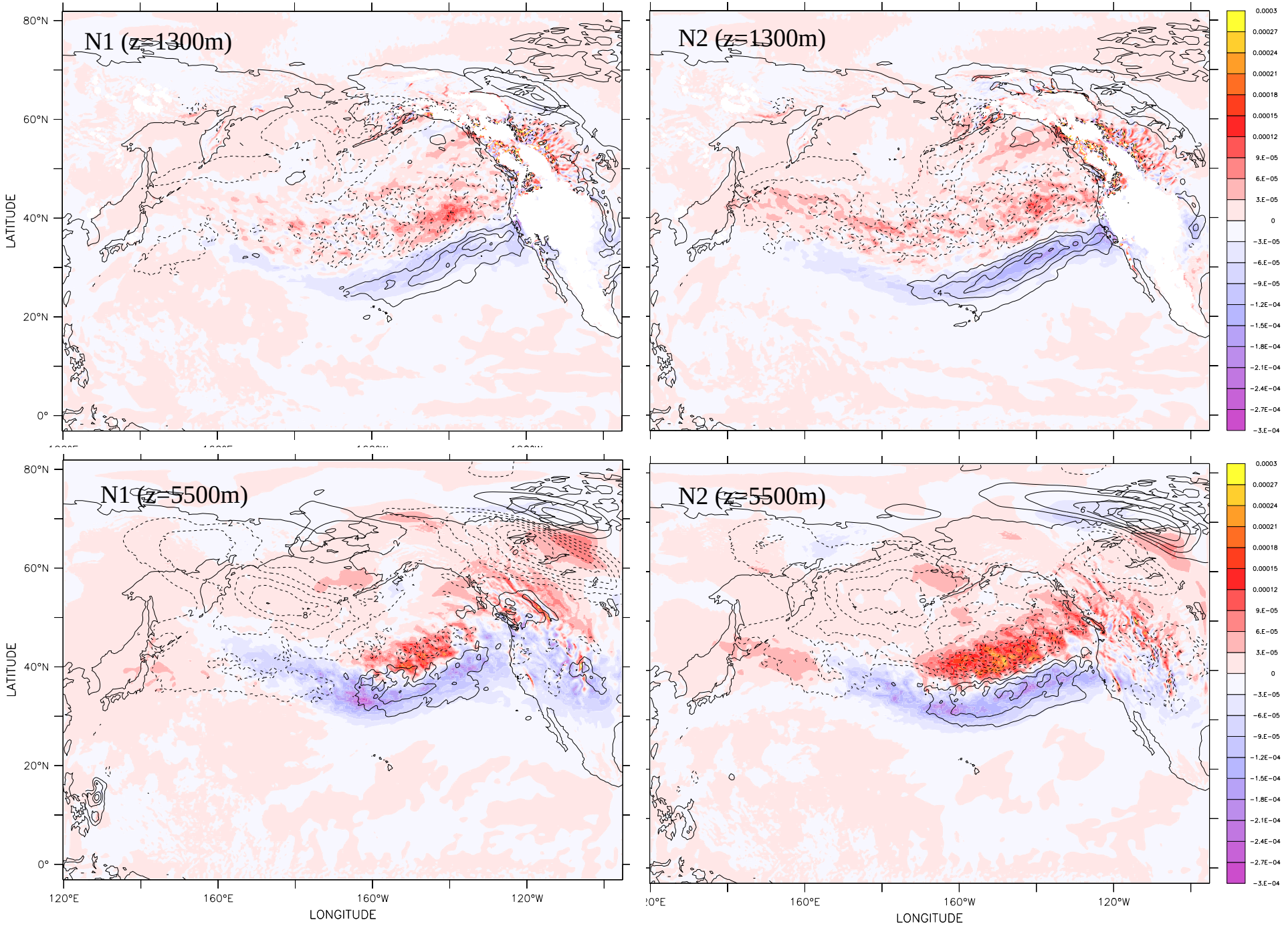

Fig 16

Barotropic Conversion (z=8900m)

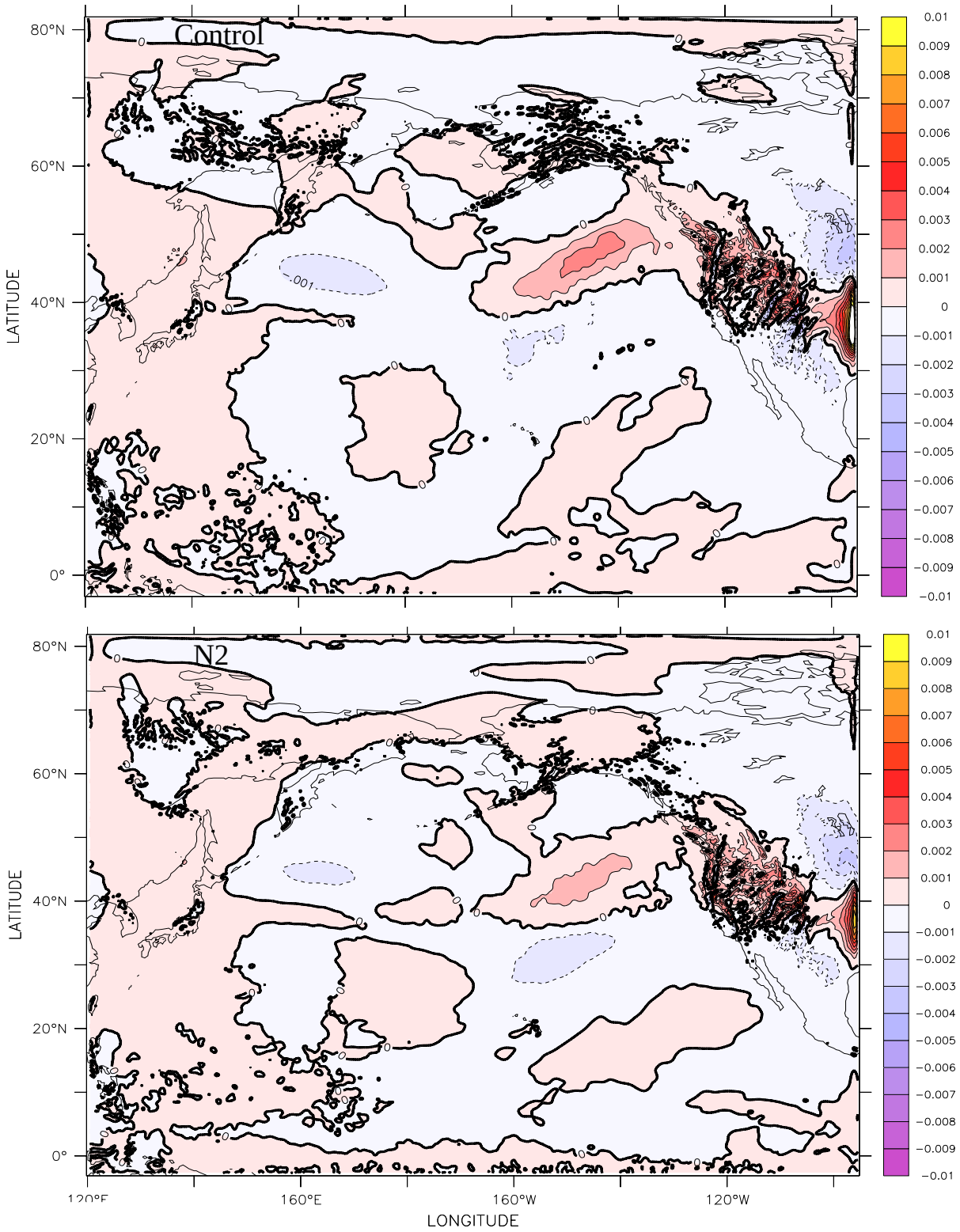

Fig 17

Baroclinic conversion (z=5500m, color) and Pressure flux (z=8900m, vector)

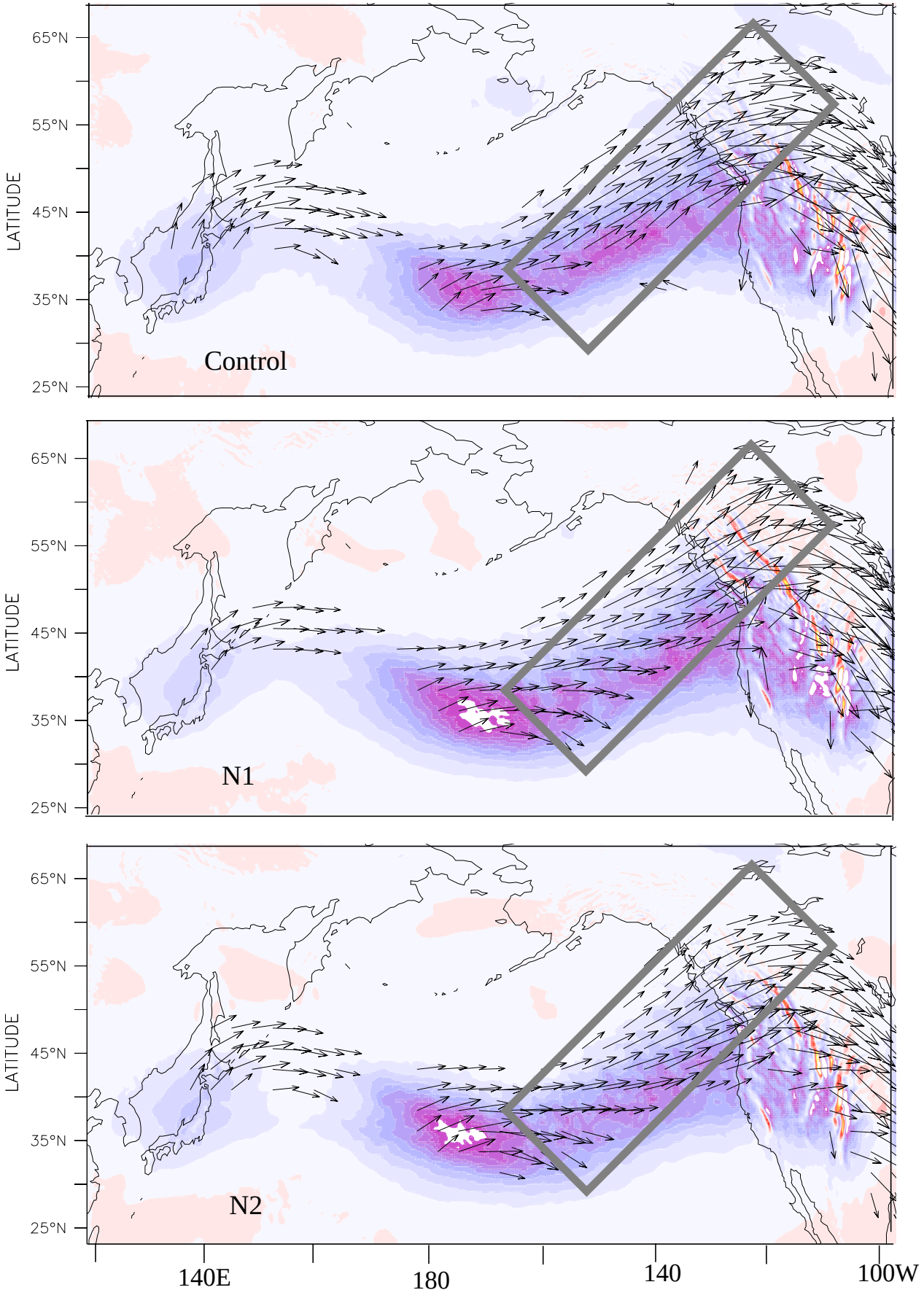

Fig 18

Potential Temperature Anomaly

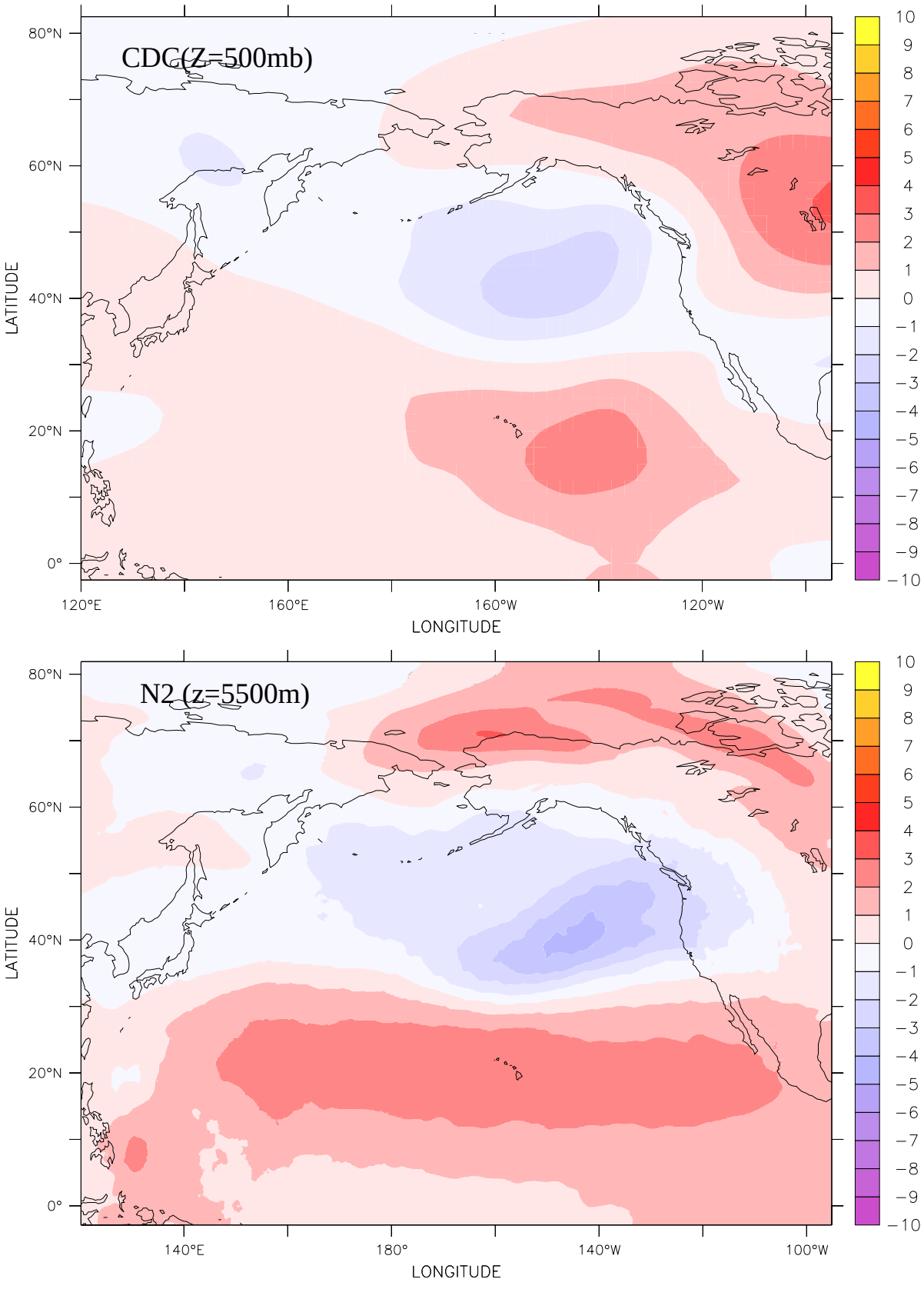

Fig 19

Cross Section of Potential Temperature , Liquid Water and Meridional Wind Vector(v,w)

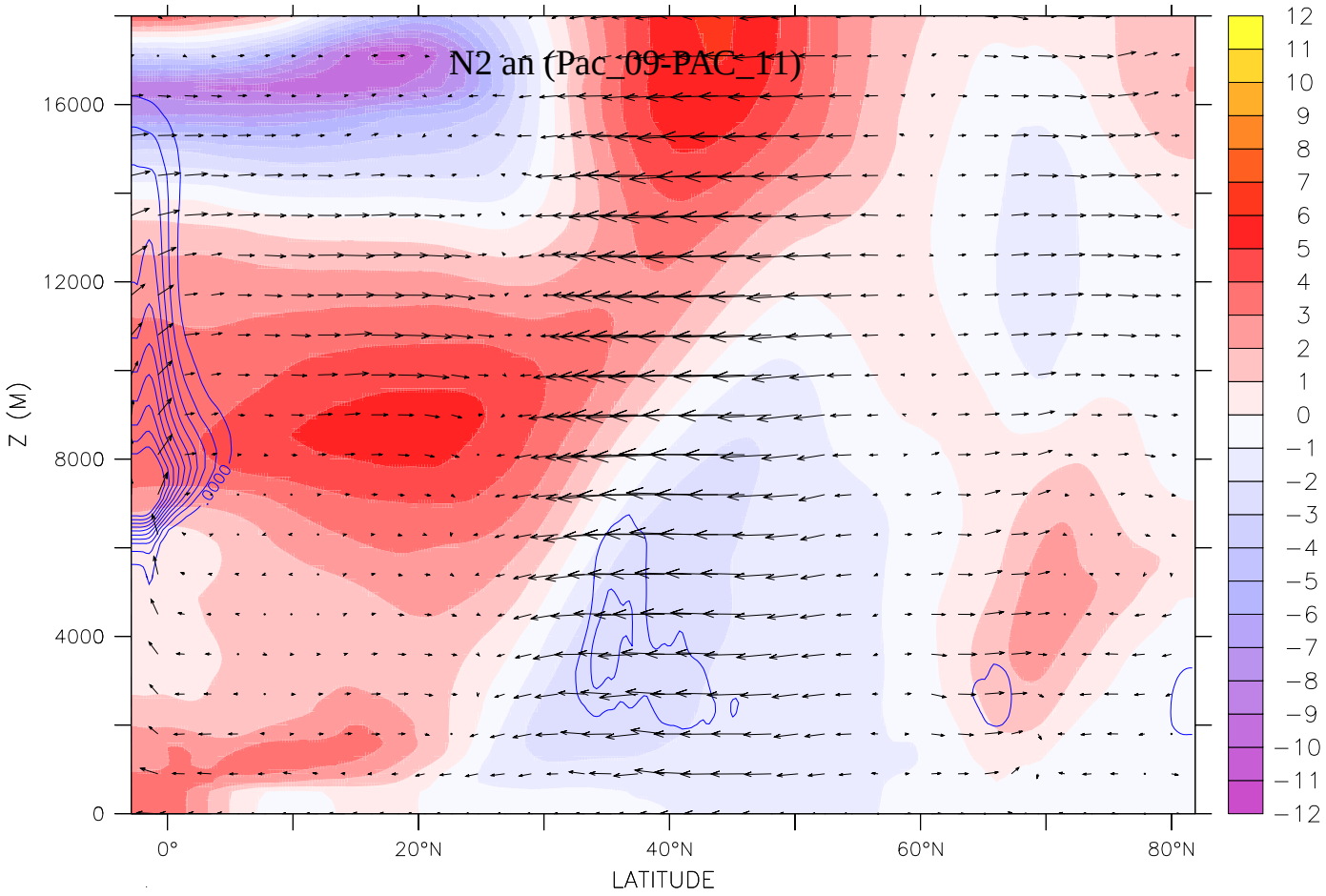

Qc an Int = 5 e-5 ⟶ 4m/s

Fig 20

Regressed Pressure (z=8900m) and Time mean Pressure deviations

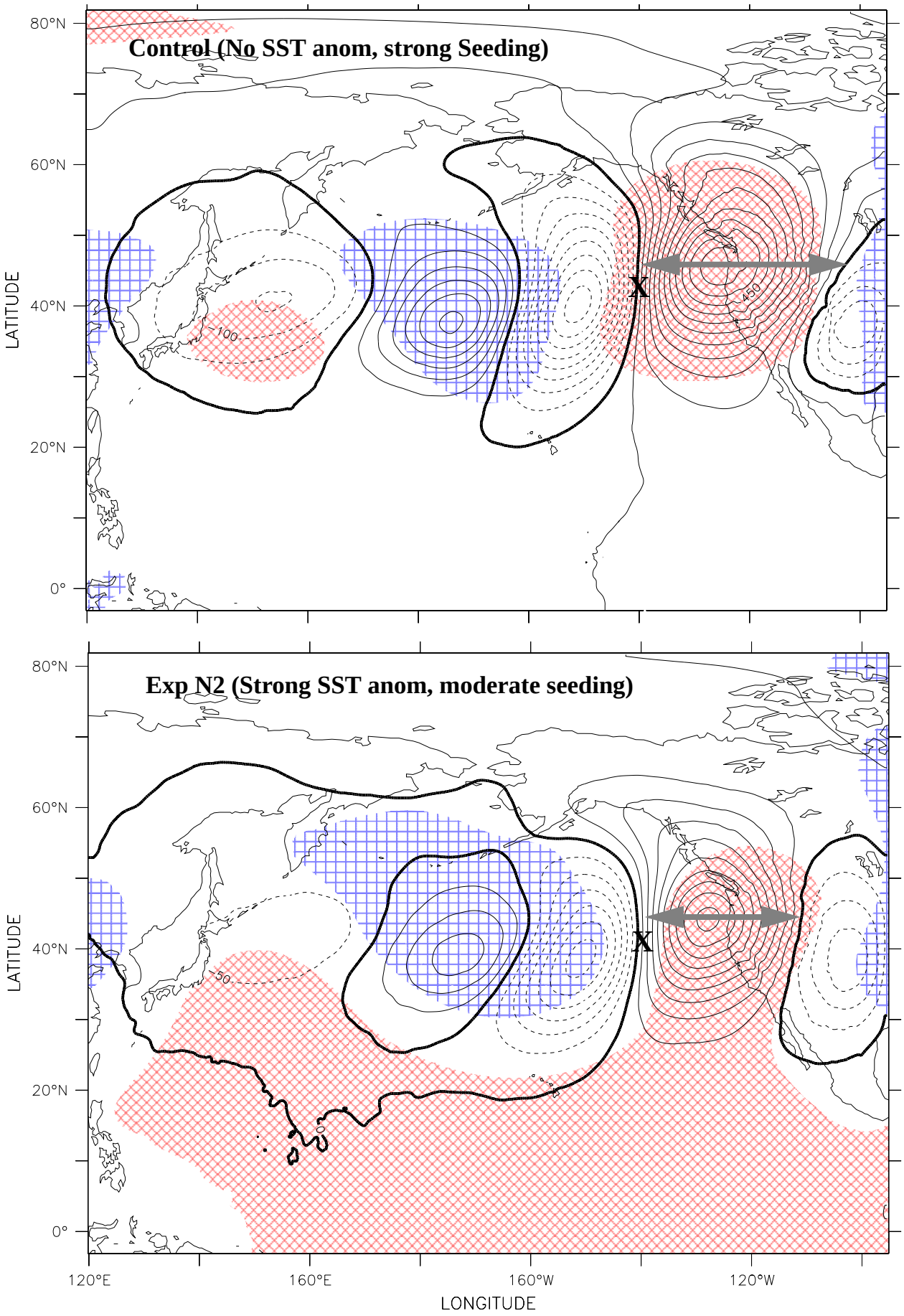

Fig 21

Hovemoller Diagram of Pressure Deviations (z=5500m) of Mean Control (averaged 30N,50N)

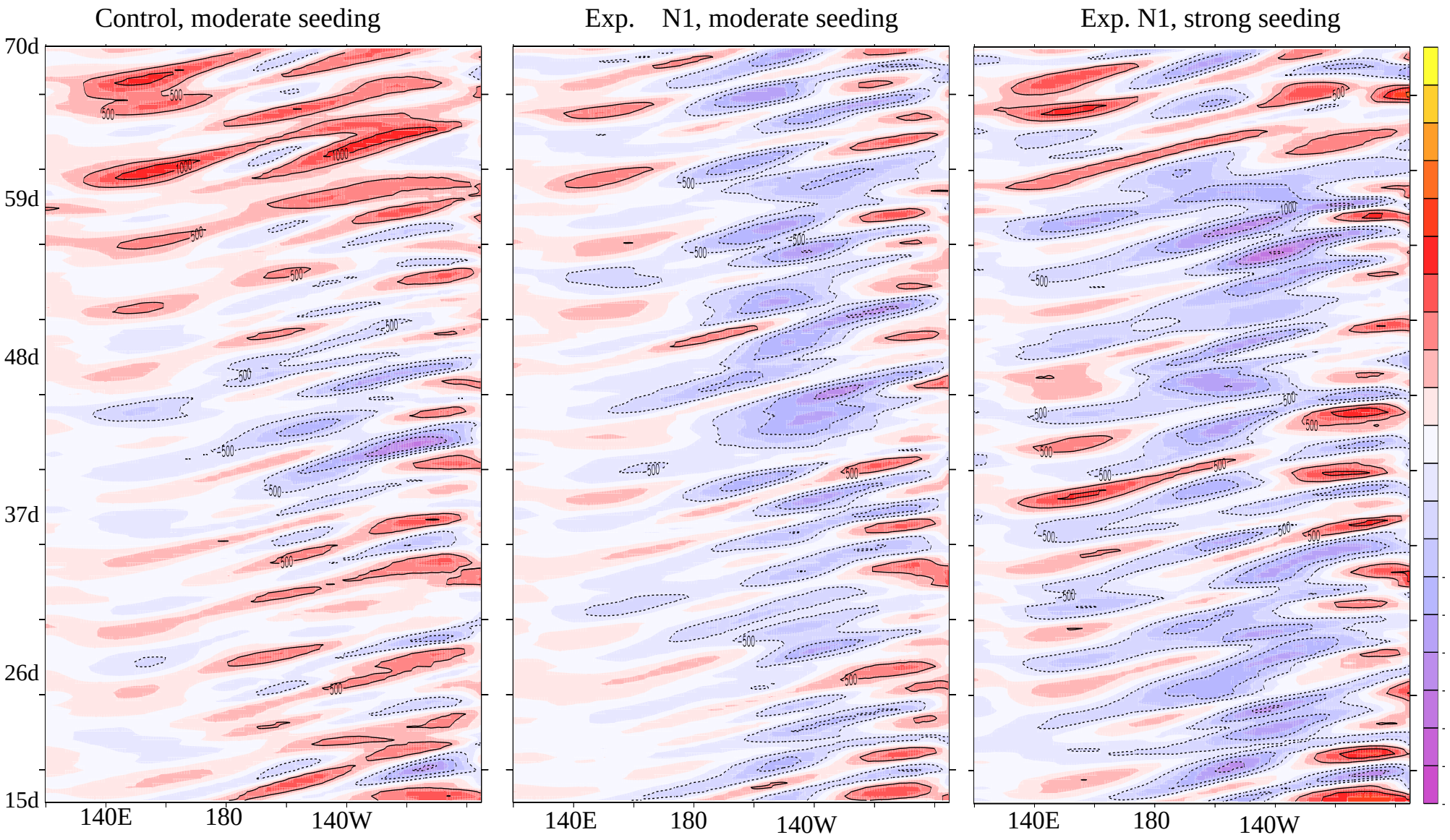

fig 22

Pressure anomaly at z= 8900m

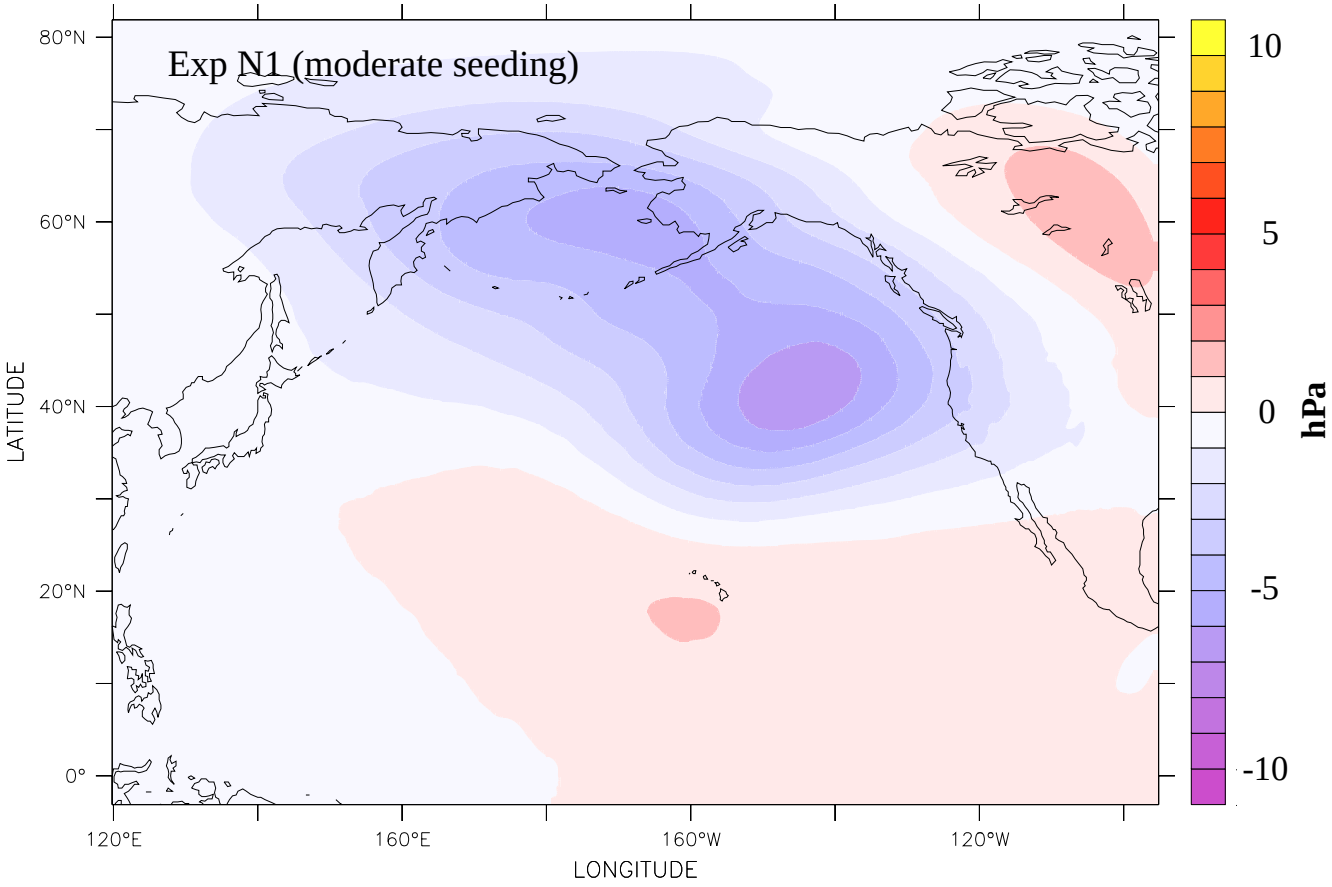

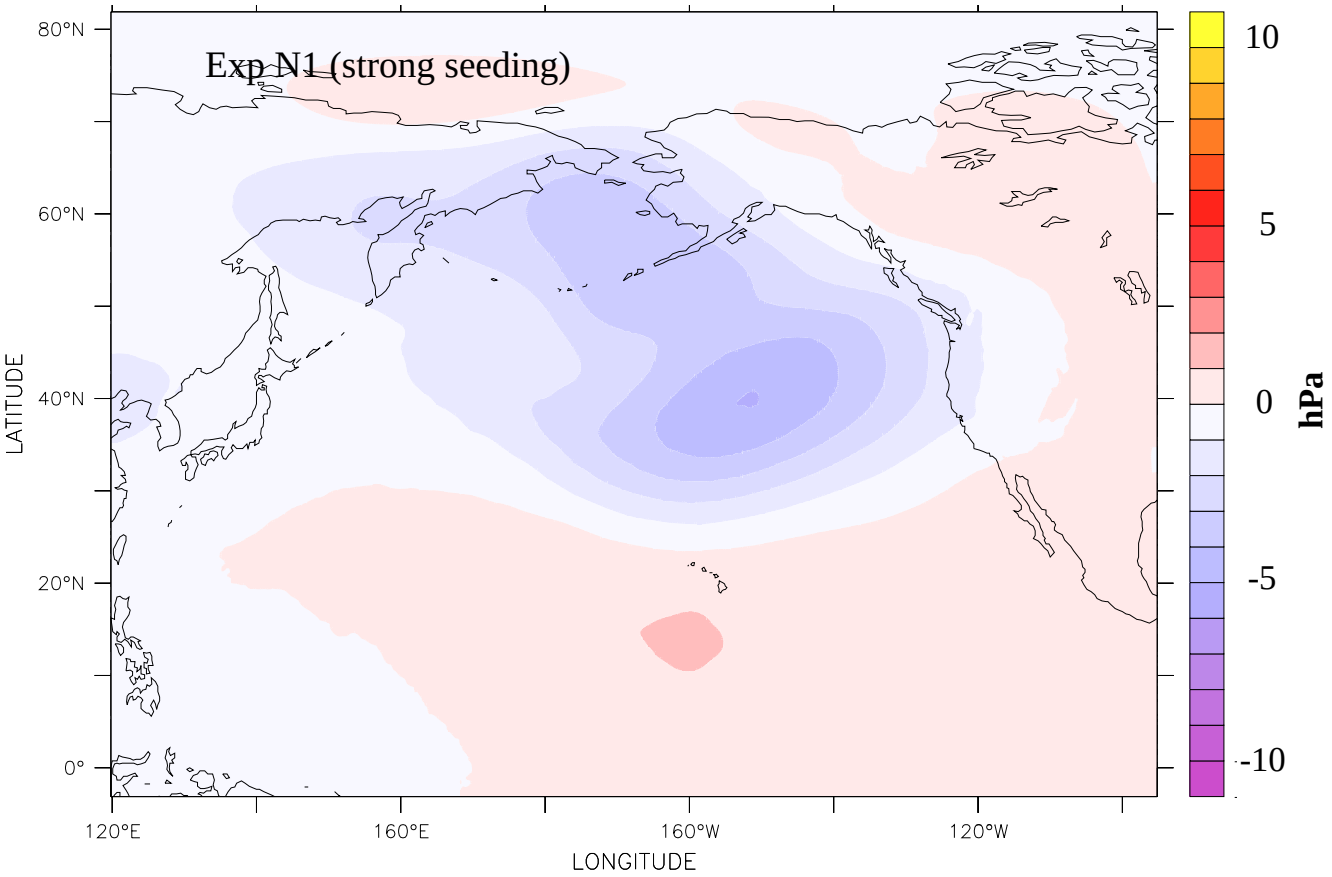

Fig 23

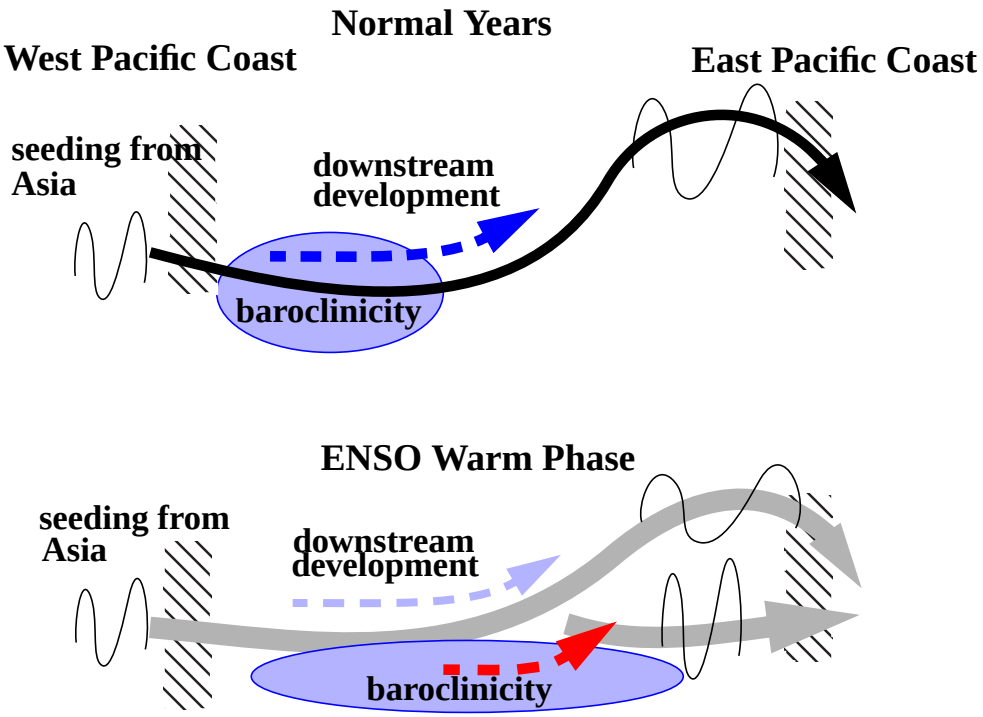
Normal Years
West Pacific Coast
East Pacific Coast
seeding from Asia
downstream development
baroclinicity
ENSO Warm Phase
seeding from Asia
downstream development
baroclinicity

Fig 24

Pacific Storm Track at Different Horizontal Resolutions
Snap-shot of Column Liquid Water Content

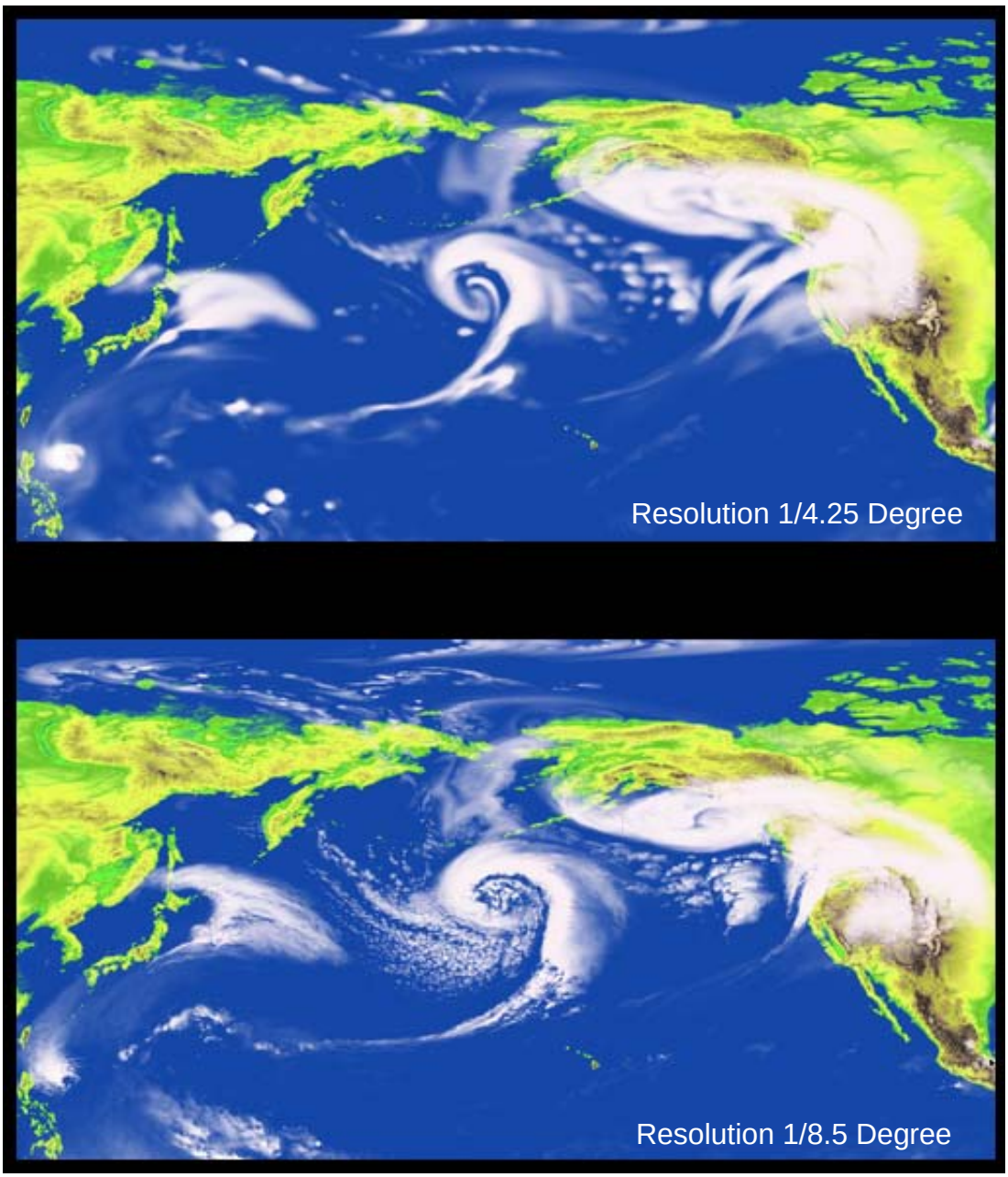

Fig A1